



# Direct and inverse spin-orbit torques

Frank Freimuth,<sup>\*</sup> Stefan Blügel, and Yuriy Mokrousov

*Peter Grünberg Institut and Institute for Advanced Simulation, Forschungszentrum Jülich and JARA, 52425 Jülich, Germany*

(Received 15 July 2014; revised manuscript received 28 July 2015; published 12 August 2015)

In collinear magnets lacking inversion symmetry, application of electric currents induces torques on the magnetization and conversely magnetization dynamics induces electric currents. The two effects, which both rely on spin-orbit interaction, are reciprocal to each other and denoted direct spin-orbit torque (SOT) and inverse spin-orbit torque (ISOT), respectively. We derive expressions for SOT and ISOT within the Kubo linear-response formalism. We show that expressions suitable for density-functional theory calculations can be derived either starting from a Kohn-Sham Hamiltonian with time-dependent exchange field or by expressing general susceptibilities in terms of the Kohn-Sham susceptibilities. For the case of magnetic bilayer systems we derive the general form of the ISOT current induced under ferromagnetic resonance. Using *ab initio* calculations within density-functional theory, we investigate SOT and ISOT in Co/Pt(111) magnetic bilayers. We determine the spatial distribution of spin and charge currents as well as torques in order to expose the mechanisms underlying SOT and ISOT and to highlight their reciprocity on the microscopic level. We find that the spin Hall effect is position dependent close to interfaces.

DOI: [10.1103/PhysRevB.92.064415](https://doi.org/10.1103/PhysRevB.92.064415)

PACS number(s): 72.25.Ba, 72.25.Mk, 71.70.Ej, 75.70.Tj

## I. INTRODUCTION

In ferromagnetic materials, Faraday's law of induction needs to be generalized to include so-called spin-motive forces, i.e., electric fields induced by the magnetization dynamics [1–3]. The spin-motive force can be interpreted as the reciprocal of the current-induced torque: A moving domain wall induces a spin-motive force and conversely an applied current drives domain-wall motion. Thus, the electric fields induced by magnetization dynamics generate a feedback effect on the magnetization via the current-induced torques which they produce [4].

Spin-motive forces do not only occur in noncollinear magnetic structures such as domain walls [5] and skyrmions [6], but can arise also in collinear magnets due to the interplay of spin orbit interaction (SOI) with bulk or structural inversion asymmetry [7,8]. Spin-orbit torques (SOTs) [9–17], i.e., current-induced torques originating from SOI in inversion-asymmetric collinear magnets, are the reciprocal to the electric fields induced by magnetization dynamics in collinear magnets [18,19]. Thus, we will denote the latter as inverse spin-orbit torques (ISOTs) in the following. ISOTs constitute a special case of spin-motive forces.

While earlier experiments on SOTs estimated the current-induced torques indirectly from the onset of nucleation of reversed domains [20] or magnetization switching at critical current densities [21–23] direct measurements of SOTs have been performed recently in bilayer systems and the SOT has been determined as a function of magnetization direction  $\hat{M}$  [24–26]. Two qualitatively different SOT components are found in these experiments on bilayer systems: the first one is an even function of  $\hat{M}$ , the second one is an odd function. Denoting the applied in-plane electric field by  $E$  and the unit vector in the out-of-plane direction by  $\hat{e}_z$ , they are given by  $T^{\text{even}} = T^{\text{even}} \hat{M} \times [(\hat{e}_z \times E) \times \hat{M}]$  and  $T^{\text{odd}} = T^{\text{odd}} (\hat{e}_z \times E) \times \hat{M}$  to lowest order in  $\hat{M}$ .

In bilayer systems based on 5d transition metals with large spin Hall effect (SHE), such as  $\text{AlO}_x/\text{Co/Pt}$ ,  $\text{MgO}/\text{CoFeB}/\text{Ta}$  and  $\text{CoFeB}/\text{W}$ , the dominant contribution to  $T^{\text{even}}$  arises from the SHE [22,23,27–31]. Conversely, in  $\text{Ni}_{80}\text{Fe}_{20}/\text{Pt}$  the spin current pumped into Pt by exciting the ferromagnetic resonance (FMR) of  $\text{Ni}_{80}\text{Fe}_{20}$  induces an electric field via the inverse spin Hall effect (ISHE) [32–34]. Rashba SOI provides an important contribution to  $T^{\text{odd}}$  in these bilayer systems [14,15]. Due to the reciprocity between SOT and ISOT, an additional ISOT is expected as well from the Rashba SOI at the bilayer interface [7,8]. This theoretical prediction, that the ISOT in bilayer systems should not arise purely from the combination of spin pumping and ISHE, is supported by the experimental observation that for the reciprocal phenomenon, the SOT,  $T^{\text{odd}}$  can be as large as or even larger than  $T^{\text{even}}$  [24–26].

So far, only the dc voltage due to FMR-driven ISOT has been studied intensively in bilayer systems [34–38]. However, after the theoretical prediction [39] that the ac component is expected to be much larger than the dc one, several recent experiments have been devoted to its measurement [40–42]. As will be discussed in this work, it is expected from the reciprocity of ISOT and SOT that the dc voltage generated by the FMR-driven ISOT is proportional to  $T^{\text{even}}$ , while the ac voltage is determined by both  $T^{\text{even}}$  and  $T^{\text{odd}}$ . Since the ac voltages associated with  $T^{\text{even}}$  and  $T^{\text{odd}}$  exhibit a phase difference of  $\pm 90^\circ$ , a nontrivial phase relationship between ac signal and magnetization trajectory is expected. Phase-sensitive measurements of the ac ISOT signal induced under FMR can thus be complementary to experiments on the SOT phenomenon. Both types of experiments, i.e., measuring the induced voltage under FMR on the one hand and measuring on the other hand the current-induced torque on the magnetization, can thus serve to determine  $T^{\text{even}}$  and  $T^{\text{odd}}$  and from them the parameters needed to model them, notably, spin-diffusion length, spin-mixing conductance, SHE angle, as well as Rashba and Dresselhaus parameters.

This paper is organized as follows: In Sec. II we discuss the Kubo formalism expressions for both SOT and ISOT. In the

<sup>\*</sup>Corresponding author: f.freimuth@fz-juelich.de

case of the SOT phenomenon, the torque on the magnetization is given by  $\mathbf{T} = \mathbf{t}\mathbf{E}$ , which defines the torkance tensor  $\mathbf{t}$ . We show that also the ISOT can be captured conveniently in terms of  $\mathbf{t}$ , which is a consequence of the reciprocity between SOT and ISOT. In Sec. II B we show that expressions for both ISOT and Gilbert damping can be derived consistently based on Kohn-Sham theory with a time-dependent exchange field. In Sec. II C we show that these expressions can also be obtained by expressing general many-body susceptibilities in terms of the corresponding Kohn-Sham susceptibilities. Exploiting the reciprocity between SOT and ISOT we then predict in Sec. III the angular dependence of ISOT in magnetic bilayers from the angular dependence of SOT recently measured in these systems. In particular, we derive and discuss the FMR-induced currents for various magnetization directions in bilayer systems. In Sec. III B a minimal model to describe even SOT and ISOT in bilayers is discussed. In Sec. III C we consider odd SOT and ISOT within the Boltzmann formalism. In Sec. IV we investigate SOT and ISOT for a magnetic bilayer composed of a Co layer on Pt(111). Computing spin currents, ISOT-induced charge currents and torkances layer resolved we make contact with phenomenological models and extract model parameters. We conclude by a summary in Sec. V.

## II. RELATIONSHIP BETWEEN DIRECT SOT AND INVERSE SOT

### A. Induced currents under time-dependent magnetization

Reciprocity between current-induced torques and spin-motive forces has been discussed in detail in the framework of phenomenological modeling [18,19,43,44]. In this section, we revisit this reciprocity on the basis of the Kubo linear-response formalism, which is well suited to study SOT and ISOT from first principles.

Within the local spin density approximation (LSDA), the interacting many-electron system is described by an effective single-particle Hamiltonian of the form

$$H(\mathbf{r}, t) = H_0(\mathbf{r}) - \mathbf{m} \cdot \hat{\mathbf{M}}(t) \Omega^{\text{xc}}(\mathbf{r}), \quad (1)$$

where the time-independent  $H_0$  contains kinetic energy, scalar potential, and SOI, while the second term on the right-hand side describes the exchange interaction.  $\hat{\mathbf{M}}(t)$  is a normalized vector which points in the direction of magnetization. In order to describe the electronic system at the ferromagnetic resonance we assume that  $\hat{\mathbf{M}}(t)$  is precessing. The time dependence of the Hamiltonian arises from this precession of magnetization.  $\mathbf{m} = -\mu_B \boldsymbol{\sigma}$  with the Bohr magneton  $\mu_B$  and the vector of Pauli spin matrices  $\boldsymbol{\sigma} = (\sigma_x, \sigma_y, \sigma_z)^T$  is the spin magnetic moment operator.  $\Omega^{\text{xc}}(\mathbf{r})$  is the exchange field, i.e., the difference between the potentials of majority and minority electrons  $\Omega^{\text{xc}}(\mathbf{r}) = \frac{1}{2\mu_B} [V_{\text{minority}}^{\text{eff}}(\mathbf{r}) - V_{\text{majority}}^{\text{eff}}(\mathbf{r})]$ . Around the time  $t$  we can approximate the motion of  $\hat{\mathbf{M}}$  by

$$\hat{\mathbf{M}}(t + \Delta t) - \hat{\mathbf{M}}(t) \simeq \frac{d\hat{\mathbf{M}}(t)}{dt} \Delta t \simeq \frac{d\hat{\mathbf{M}}(t)}{dt} \frac{\sin(\omega \Delta t)}{\omega} \quad (2)$$

for small time changes  $\Delta t$  and a small but arbitrary frequency  $\omega$  with  $\omega \Delta t \ll 1$ . Likewise, the Hamiltonian can be

approximated as

$$H(\mathbf{r}, t + \Delta t) \simeq H(\mathbf{r}, t) - \mathbf{m} \cdot \frac{d\hat{\mathbf{M}}(t)}{dt} \Omega^{\text{xc}}(\mathbf{r}) \frac{\sin(\omega \Delta t)}{\omega}. \quad (3)$$

The  $\Delta t$ -dependent term

$$\begin{aligned} V(\mathbf{r}, \Delta t) &= -\mathbf{m} \cdot \frac{d\hat{\mathbf{M}}(t)}{dt} \Omega^{\text{xc}}(\mathbf{r}) \frac{\sin(\omega \Delta t)}{\omega} \\ &= -\mathbf{m} \cdot \left[ \hat{\mathbf{M}}(t) \times \left( \frac{d\hat{\mathbf{M}}(t)}{dt} \times \hat{\mathbf{M}}(t) \right) \right] \Omega^{\text{xc}}(\mathbf{r}) \frac{\sin(\omega \Delta t)}{\omega} \\ &= \frac{\sin(\omega \Delta t)}{\omega} \left( \hat{\mathbf{M}}(t) \times \frac{d\hat{\mathbf{M}}(t)}{dt} \right) \cdot \mathcal{T}(\mathbf{r}, t) \end{aligned} \quad (4)$$

acts as a time-dependent perturbation on the eigenstates of  $H(\mathbf{r}, t)$ . Here,  $\mathcal{T}(\mathbf{r}, t) = \mathbf{m} \times \hat{\mathbf{M}}(t) \Omega^{\text{xc}}(\mathbf{r})$  is the torque operator.

Within linear response, the current density in  $\alpha$  direction  $j_\alpha$ , induced by the time-dependent perturbation Eq. (4), is given by

$$j_\alpha(t) = \sum_\beta \frac{e}{V} \lim_{\omega \rightarrow 0} \frac{\text{Im} G_{v_\alpha, \mathcal{T}_\beta}^R[\hbar\omega, \hat{\mathbf{M}}(t)]}{\hbar\omega} \left( \hat{\mathbf{M}}(t) \times \frac{d\hat{\mathbf{M}}(t)}{dt} \right)_\beta, \quad (5)$$

where  $e > 0$  is the elementary positive charge,  $V$  is the volume, and  $G_{v_\alpha, \mathcal{T}_\beta}^R(\hbar\omega, \hat{\mathbf{M}})$  is the Fourier transform of the retarded velocity-torque correlation function, i.e.,

$$G_{v_\alpha, \mathcal{T}_\beta}^R(\hbar\omega, \hat{\mathbf{M}}) = -i \int_0^\infty dt e^{i\omega t} \langle [v_\alpha(t), \mathcal{T}_\beta(0)]_- \rangle, \quad (6)$$

evaluated for the time-independent Hamiltonian

$$H_{\hat{\mathbf{M}}}(\mathbf{r}) = H_0(\mathbf{r}) - \mathbf{m} \cdot \hat{\mathbf{M}} \Omega^{\text{xc}}(\mathbf{r}) \quad (7)$$

of a system with magnetization in direction  $\hat{\mathbf{M}} = \hat{\mathbf{M}}(t)$ . Equation (6) describes the correlation between the polar vector  $\mathbf{v}$  and the axial vector  $\mathcal{T}$ . This polar-axial correlation is nonzero only when inversion symmetry is broken.

Next, we compare Eq. (5) to the expressions describing SOTs. Within linear response to an applied electric field  $\mathbf{E}$  the SOT on the magnetization is  $\mathbf{T}(\hat{\mathbf{M}}) = \mathbf{t}(\hat{\mathbf{M}})\mathbf{E}$ , where the torkance tensor  $\mathbf{t}(\hat{\mathbf{M}})$  is given by [31,45]

$$t_{\alpha\beta}(\hat{\mathbf{M}}) = -e \lim_{\omega \rightarrow 0} \frac{\text{Im} G_{\mathcal{T}_\alpha, v_\beta}^R(\hbar\omega, \hat{\mathbf{M}})}{\hbar\omega} \quad (8)$$

in terms of the Fourier transform of the retarded torque-velocity correlation function

$$G_{\mathcal{T}_\alpha, v_\beta}^R(\hbar\omega, \hat{\mathbf{M}}) = -i \int_0^\infty dt e^{i\omega t} \langle [\mathcal{T}_\alpha(t), v_\beta(0)]_- \rangle \quad (9)$$

of the system with Hamiltonian (7).

The spectral densities of the Green functions defined in Eqs. (6) and (9) are given by

$$\begin{aligned} S_{v_\alpha, \mathcal{T}_\beta}(t, t', \hat{\mathbf{M}}) &= \frac{1}{2\pi} \langle [v_\alpha(t), \mathcal{T}_\beta(t')]_- \rangle, \\ S_{\mathcal{T}_\alpha, v_\beta}(t, t', \hat{\mathbf{M}}) &= \frac{1}{2\pi} \langle [\mathcal{T}_\alpha(t), v_\beta(t')]_- \rangle \end{aligned} \quad (10)$$

and their Fourier transforms satisfy the relations

$$\begin{aligned} S_{\mathcal{T}_\alpha, v_\beta}(\hbar\omega, \hat{\mathbf{M}}) &= [S_{v_\beta, \mathcal{T}_\alpha}(\hbar\omega, \hat{\mathbf{M}})]^*, \\ \text{Re}[S_{v_\beta, \mathcal{T}_\alpha}(\hbar\omega, -\hat{\mathbf{M}})] &= -\text{Re}[S_{v_\beta, \mathcal{T}_\alpha}(\hbar\omega, \hat{\mathbf{M}})], \\ \text{Im}[S_{v_\beta, \mathcal{T}_\alpha}(\hbar\omega, -\hat{\mathbf{M}})] &= \text{Im}[S_{v_\beta, \mathcal{T}_\alpha}(\hbar\omega, \hat{\mathbf{M}})], \end{aligned} \quad (11)$$

from which follows

$$S_{\mathcal{T}_\alpha, v_\beta}(\hbar\omega, \hat{\mathbf{M}}) = -S_{v_\beta, \mathcal{T}_\alpha}(\hbar\omega, -\hat{\mathbf{M}}) \quad (12)$$

and thus

$$G_{\mathcal{T}_\alpha, v_\beta}^R(\hbar\omega, \hat{\mathbf{M}}) = -G_{v_\beta, \mathcal{T}_\alpha}^R(\hbar\omega, -\hat{\mathbf{M}}). \quad (13)$$

This identity allows us to rewrite the magnetization-dynamics-induced current density [Eq. (5)] in terms of the torkance tensor as

$$j_\alpha(t) = \frac{1}{V} \sum_\beta t_{\beta\alpha}(-\hat{\mathbf{M}}(t)) \left( \hat{\mathbf{M}}(t) \times \frac{d\hat{\mathbf{M}}(t)}{dt} \right)_\beta. \quad (14)$$

Equation (14) is the central result of this section. It shows that it is very convenient to discuss the ISOT in terms of the very same torkance tensor  $\mathbf{t}$  as the SOT. We note in passing that the torque-velocity correlations, which the torkance measures, govern also the Dzyaloshinskii-Moriya interaction [45,46].

It is convenient to decompose the torkance tensor into two components that are even and odd with respect to magnetization reversal, respectively [31]:  $\mathbf{t}(\hat{\mathbf{M}}) = \mathbf{t}^{\text{even}}(\hat{\mathbf{M}}) + \mathbf{t}^{\text{odd}}(\hat{\mathbf{M}})$ , where  $\mathbf{t}^{\text{even}}(\hat{\mathbf{M}}) = [\mathbf{t}(\hat{\mathbf{M}}) + \mathbf{t}(-\hat{\mathbf{M}})]/2$  and  $\mathbf{t}^{\text{odd}}(\hat{\mathbf{M}}) = [\mathbf{t}(\hat{\mathbf{M}}) - \mathbf{t}(-\hat{\mathbf{M}})]/2$ . Separating  $j_\alpha$  into the components due to  $\mathbf{t}^{\text{even}}(\hat{\mathbf{M}})$  and  $\mathbf{t}^{\text{odd}}(\hat{\mathbf{M}})$  yields

$$\begin{aligned} j_\alpha^{\text{even}}(t) &= \frac{1}{V} \sum_\beta t_{\beta\alpha}^{\text{even}}(\hat{\mathbf{M}}(t)) \left( \hat{\mathbf{M}}(t) \times \frac{d\hat{\mathbf{M}}(t)}{dt} \right)_\beta, \\ j_\alpha^{\text{odd}}(t) &= -\frac{1}{V} \sum_\beta t_{\beta\alpha}^{\text{odd}}(\hat{\mathbf{M}}(t)) \left( \hat{\mathbf{M}}(t) \times \frac{d\hat{\mathbf{M}}(t)}{dt} \right)_\beta. \end{aligned} \quad (15)$$

### B. Completing the response matrix

When the electronic system is perturbed due to the time dependence of the exchange field direction, a current density is induced according to Eq. (5). This induced electric current is not the only response of the electrons to this time-dependent perturbation: Additionally, the torque  $-V \mathbf{\Lambda}(\hat{\mathbf{M}} \times \frac{d\hat{\mathbf{M}}}{dt})$  acts on the magnetization, where

$$\Lambda_{\alpha\beta} = -\frac{1}{V} \lim_{\omega \rightarrow 0} \frac{\text{Im} G_{\mathcal{T}_\alpha, \mathcal{T}_\beta}^R(\hbar\omega, \hat{\mathbf{M}})}{\hbar\omega}. \quad (16)$$

The sum of all torques on the magnetization has to be zero from the point of view of an observer that rotates together with the magnetization:

$$0 = \mathbf{tE} - V \mathbf{\Lambda} \left( \hat{\mathbf{M}} \times \frac{d\hat{\mathbf{M}}}{dt} \right) + \mu_0 M V \hat{\mathbf{M}} \times \mathbf{H}^{\text{eff}}. \quad (17)$$

Here, the first term on the right-hand side is the SOT. Torques such as the Gilbert damping torque, which are exerted on the magnetization due to the magnetization dynamics, are described by the second term. The third term summarizes

torques due to external magnetic fields and due to magnetic anisotropy.  $\mathbf{M}$  in the third term is the magnetization, i.e.,  $MV$  is the magnetic moment. In the presence of SOTs, the extended Landau-Lifshitz-Gilbert equation runs

$$\frac{d\hat{\mathbf{M}}}{dt} = -|\gamma| \hat{\mathbf{M}} \times \mathbf{H}^{\text{eff}} + \alpha \hat{\mathbf{M}} \times \frac{d\hat{\mathbf{M}}}{dt} - \frac{|\gamma| \mathbf{tE}}{\mu_0 M V}, \quad (18)$$

where  $\gamma = g\mu_0\mu_B/\hbar$  is the gyromagnetic ratio and  $\alpha$  is the Gilbert damping tensor. Comparison of Eqs. (18) and (17) leads to

$$\frac{1}{\gamma} = \frac{1}{2\mu_0 M} \sum_{\alpha\beta\delta} \epsilon_{\alpha\beta\delta} \Lambda_{\alpha\beta}^{\text{odd}} \hat{M}_\delta, \quad (19)$$

where  $\epsilon_{\alpha\beta\delta}$  is the Levi-Civita symbol, and

$$\alpha = \frac{|\gamma| \mathbf{\Lambda}^{\text{even}}}{M \mu_0}. \quad (20)$$

It is straightforward to show that Eq. (20) combined with Eq. (16) reproduces the Gilbert damping expressions used within *ab initio* calculations [47]. In the absence of SOI, it is found that [48]

$$\Lambda_{\alpha\beta}^{\text{odd}} = -\frac{\hbar}{2\mu_B} \sum_\gamma \epsilon_{\alpha\beta\gamma} M_\gamma. \quad (21)$$

Inserting this result into Eq. (19) leads to the expected nonrelativistic value of  $\gamma = -\frac{2\mu_0\mu_B}{\hbar}$  and  $g = -2$ .

If we consider the coupled problem where both the electric field and the magnetization dynamics drive both the electric current and induce torques, the even torkance  $\mathbf{t}^{\text{even}}$  determines the off-diagonal elements of the symmetric part  $\mathbf{A}^s$  of the corresponding linear-response matrix, while the odd torkance  $\mathbf{t}^{\text{odd}}$  determines those of the antisymmetric part  $\mathbf{A}^a$ :

$$\begin{aligned} \begin{pmatrix} \mathbf{j} \\ \mathbf{T}/V \end{pmatrix} &= [\mathbf{A}^s(\hat{\mathbf{M}}) + \mathbf{A}^a(\hat{\mathbf{M}})] \begin{pmatrix} \mathbf{E} \\ \hat{\mathbf{M}} \times \frac{d\hat{\mathbf{M}}}{dt} \end{pmatrix}, \\ \mathbf{A}^s(\hat{\mathbf{M}}) &= \begin{pmatrix} \boldsymbol{\sigma}^{\text{even}}(\hat{\mathbf{M}}) & [\mathbf{t}^{\text{even}}(\hat{\mathbf{M}})]^T/V \\ \mathbf{t}^{\text{even}}(\hat{\mathbf{M}})/V & -\mathbf{\Lambda}^{\text{even}}(\hat{\mathbf{M}}) \end{pmatrix}, \\ \mathbf{A}^a(\hat{\mathbf{M}}) &= \begin{pmatrix} \boldsymbol{\sigma}^{\text{odd}}(\hat{\mathbf{M}}) & -[\mathbf{t}^{\text{odd}}(\hat{\mathbf{M}})]^T/V \\ \mathbf{t}^{\text{odd}}(\hat{\mathbf{M}})/V & -\mathbf{\Lambda}^{\text{odd}}(\hat{\mathbf{M}}) \end{pmatrix}. \end{aligned} \quad (22)$$

Here,  $\boldsymbol{\sigma}$  is the tensor of electrical conductivity. The torque  $\mathbf{T}$  in the first equation, i.e.,  $\mathbf{T} = \mathbf{tE} - V \mathbf{\Lambda}(\hat{\mathbf{M}} \times \frac{d\hat{\mathbf{M}}}{dt})$ , is the torque on the magnetization due to the response of the electrons to the two perturbations  $\mathbf{E}$  and  $\frac{d\hat{\mathbf{M}}}{dt}$ . According to Eq. (17), the sum of this torque and the torques due to magnetic anisotropy and external magnetic fields is zero. Due to the Onsager relation  $\sigma_{\alpha\beta}(\hat{\mathbf{M}}) = \sigma_{\beta\alpha}(-\hat{\mathbf{M}})$  the even part of the conductivity tensor is symmetric, i.e.,  $\sigma_{\alpha\beta}^{\text{even}}(\hat{\mathbf{M}}) = \sigma_{\beta\alpha}^{\text{even}}(\hat{\mathbf{M}})$ , while the odd part is antisymmetric, i.e.,  $\sigma_{\alpha\beta}^{\text{odd}}(\hat{\mathbf{M}}) = -\sigma_{\beta\alpha}^{\text{odd}}(\hat{\mathbf{M}})$  [49]. Similarly,  $\Lambda_{\alpha\beta}^{\text{even}}(\hat{\mathbf{M}}) = \Lambda_{\beta\alpha}^{\text{even}}(\hat{\mathbf{M}})$  and  $\Lambda_{\alpha\beta}^{\text{odd}}(\hat{\mathbf{M}}) = -\Lambda_{\beta\alpha}^{\text{odd}}(\hat{\mathbf{M}})$ . Consequently,  $\mathbf{A}^s(\hat{\mathbf{M}})$  is indeed symmetric and additionally even with respect to magnetization reversal. Likewise,  $\mathbf{A}^a(\hat{\mathbf{M}})$  is indeed antisymmetric and additionally odd with respect to magnetization reversal. Therefore, the linear-response matrix  $\mathbf{A}(\hat{\mathbf{M}}) = \mathbf{A}^s(\hat{\mathbf{M}}) + \mathbf{A}^a(\hat{\mathbf{M}})$  satisfies the symmetry

$$(\mathbf{A}(\hat{\mathbf{M}}))^T = \mathbf{A}(-\hat{\mathbf{M}}), \quad (23)$$

which summarizes the Onsager relations of  $\sigma$ ,  $\Lambda$ , and  $t$  in a compact form.

Equations (16) and (22) are the central results of this section. They show that Gilbert damping  $\alpha$  [Eq. (20)], gyromagnetic ratio  $\gamma$  [Eq. (19)], as well as ISOT [Eq. (5)] can be extracted coherently and consistently from time-dependent perturbation theory, where the perturbation due to magnetization dynamics is given by Eq. (4).

From the point of view of adiabatic electron dynamics in a time-dependent Hamiltonian (1), it is natural to consider the precession of the exchange field as perturbation. The electronic system responds to this perturbation by the ISOT current [Eq. (5)]. Additionally, it responds by the torque  $\mathbf{T} = -V\Lambda(\hat{\mathbf{M}} \times \frac{d\hat{\mathbf{M}}}{dt})$  described by Eq. (16). However, when the Onsager reciprocity principle is used to relate SOT and ISOT in a phenomenological approach, typically a different point of view is taken: The effective magnetic field  $\mathbf{H}^{\text{eff}}$  is considered as a thermodynamic force and the time derivative of magnetization plays the role of the associated thermodynamic flux [19]. Instead of considering the response of  $(\mathbf{j}, \mathbf{T}/V)^T$  to the perturbation  $(\mathbf{E}, \hat{\mathbf{M}} \times \frac{d\hat{\mathbf{M}}}{dt})^T$  as we do in Eq. (22), one considers then instead the response of the thermodynamic fluxes  $(\frac{d\hat{\mathbf{M}}}{dt}, \mathbf{j})^T$  to the thermodynamic forces  $(\mathbf{H}^{\text{eff}}, \mathbf{E})^T$ . Interestingly,  $\frac{d\hat{\mathbf{M}}}{dt}$  appears then as a response rather than as a perturbation. However, both formulations of the reciprocity between SOT and ISOT are equivalent.

### C. Many-electron response functions

In the previous two subsections we discussed SOT and ISOT based on the effective single-particle Hamiltonian defined in Eq. (1), where the exchange field  $\Omega^{\text{xc}}(\mathbf{r})$  needs to be obtained self-consistently within LSDA. In this section, we consider SOT and ISOT from the interacting many-electron point of view.

When a small static electric field  $\mathbf{E}$  is applied to a magnet with broken inversion symmetry, its magnetization will assume a new direction  $\hat{\mathbf{M}} + \delta\hat{\mathbf{M}}$  due to the action of the SOT. We assume that  $\mathbf{E}$  is sufficiently small to ensure that the magnetization is not switched and that  $\hat{\mathbf{M}} + \delta\hat{\mathbf{M}}$  is time independent. Within linear response the relation between  $\delta\hat{\mathbf{M}}$  and  $\mathbf{E}$  is given by

$$\delta\hat{\mathbf{M}} = \frac{1}{MV} \Xi(\hat{\mathbf{M}}) \mathbf{E} \quad (24)$$

with

$$\Xi_{\alpha\beta}(\hat{\mathbf{M}}) = \lim_{\omega \rightarrow 0} \frac{e}{i\omega\hbar} \mathcal{G}_{m_\alpha, v_\beta}^R(\hbar\omega, \hat{\mathbf{M}}), \quad (25)$$

where

$$\mathcal{G}_{m_\alpha, v_\beta}^R(\hbar\omega, \hat{\mathbf{M}}) = -i \int_0^\infty dt e^{i\omega t} \langle [m_\alpha(t), v_\beta(0)]_- \rangle \quad (26)$$

is the retarded spin-moment velocity correlation function. While the correlation functions defined in Eqs. (6), (9), and (16) are evaluated based on the Kohn-Sham eigenfunctions of the effective single-particle Hamiltonian (7), Eq. (26) has to be evaluated based on the interacting many-electron wave

functions of the system, i.e.,

$$\mathcal{G}_{m_\alpha, v_\beta}^R(\hbar\omega, \hat{\mathbf{M}}) = \sum_n \hbar \left[ \frac{\langle \Psi_0 | m_\alpha | \Psi_n \rangle \langle \Psi_n | v_\beta | \Psi_0 \rangle}{\mathcal{E}_0 - \mathcal{E}_n + \hbar\omega + i\eta} - \frac{\langle \Psi_0 | v_\beta | \Psi_n \rangle \langle \Psi_n | m_\alpha | \Psi_0 \rangle}{\mathcal{E}_n - \mathcal{E}_0 + \hbar\omega + i\eta} \right], \quad (27)$$

where  $\Psi_0$  is the ground state and  $\Psi_n$  with  $n > 0$  are the excited states. The energies of the ground state and of the excited states are  $\mathcal{E}_0$  and  $\mathcal{E}_n$ , respectively. We use the symbol  $\mathcal{G}^R$  to denote the retarded many-electron response functions while we use  $G^R$  to denote the retarded Kohn-Sham single-particle response functions.

We can quantify the SOT that gives rise to the rotation of magnetization  $\delta\hat{\mathbf{M}}$  in Eq. (24) in terms of the magnetic field  $\mathbf{H}^{\text{SOT}}$  that would need to be applied perpendicular to  $\hat{\mathbf{M}}$  to achieve the same tilt  $\delta\hat{\mathbf{M}}$  without applied electric field  $\mathbf{E}$ . The relation between  $\delta\hat{\mathbf{M}}$  and  $\mathbf{H}^{\text{SOT}}$  is described by the transverse magnetic susceptibility  $\chi$ :

$$M\delta\hat{\mathbf{M}} = \chi(\hat{\mathbf{M}}) \mathbf{H}^{\text{SOT}}, \quad (28)$$

where

$$\chi_{\alpha\beta}(\hat{\mathbf{M}}) = -\frac{\mu_0}{V\hbar} \mathcal{G}_{m_\alpha, m_\beta}^R(\hbar\omega = 0, \hat{\mathbf{M}}). \quad (29)$$

The static transverse magnetic susceptibility  $\chi(\hat{\mathbf{M}})$  contains the information on the magnetic anisotropy [50]: When the magnetization is tilted away from the easy axis due to the applied transverse magnetic field  $\mathbf{H}^{\text{SOT}}$ , the additional internal magnetic field

$$\mathbf{H}^{\text{MAE}} = -M[\chi(\hat{\mathbf{M}})]^{-1} \delta\hat{\mathbf{M}} \quad (30)$$

due to magnetic anisotropy acts on the magnetization. The tilt  $\delta\hat{\mathbf{M}}$  is such that  $\mathbf{H}^{\text{MAE}} + \mathbf{H}^{\text{SOT}} = 0$ . Equating the right-hand sides of Eqs. (24) and (28) we obtain an expression for the magnetic field  $\mathbf{H}^{\text{SOT}}$ :

$$\mathbf{H}^{\text{SOT}} = \frac{1}{V} [\chi(\hat{\mathbf{M}})]^{-1} \Xi(\hat{\mathbf{M}}) \mathbf{E}. \quad (31)$$

This magnetic field exerts the torque  $\mu_0 M V \hat{\mathbf{M}} \times \mathbf{H}^{\text{SOT}}$  on the magnetization. Exactly the same torque acts on the magnetization when the electric field  $\mathbf{E}$  is applied instead of the magnetic field  $\mathbf{H}^{\text{SOT}}$ , i.e., the SOT is given by  $\mu_0 M V \hat{\mathbf{M}} \times \mathbf{H}^{\text{SOT}}$ . The corresponding torque can be written as

$$\tilde{t}(\hat{\mathbf{M}}) = \mu_0 M \hat{\mathbf{M}} \times [\chi(\hat{\mathbf{M}})]^{-1} \Xi(\hat{\mathbf{M}}). \quad (32)$$

The applicability of Eq. (8) is restricted to LSDA because it is based on the torque operator  $\mathcal{T}$  and hence on the exchange field  $\Omega^{\text{xc}}(\mathbf{r})$ . In contrast, Eq. (32) provides a general formulation of the torque.

In order to show that Eq. (32) reduces to Eq. (8) within LSDA, i.e.,  $\tilde{t}(\hat{\mathbf{M}}) = t(\hat{\mathbf{M}})$ , we need to express the many-electron response functions  $\Xi(\hat{\mathbf{M}})$  and  $\chi(\hat{\mathbf{M}})$  through the corresponding single-particle Kohn-Sham response functions

$$\Xi_{\alpha\beta}^{\text{KS}}(\hat{\mathbf{M}}, \mathbf{r}) = \lim_{\omega \rightarrow 0} \frac{e}{i\omega\hbar} G_{m_\alpha(\mathbf{r}), v_\beta}^R(\hbar\omega, \hat{\mathbf{M}}) \quad (33)$$

and

$$\chi_{\alpha\beta}^{\text{KS}}(\hat{\mathbf{M}}, \mathbf{r}, \mathbf{r}') = -\frac{\mu_0}{\hbar} G_{m_\alpha(\mathbf{r}), m_\beta(\mathbf{r}')}^R(\hbar\omega = 0, \hat{\mathbf{M}}), \quad (34)$$



where  $m_\alpha(\mathbf{r})$  is the operator of spin magnetic moment density at position  $\mathbf{r}$ , i.e.,  $\int d^3r m_\alpha(\mathbf{r}) = m_\alpha = -\mu_B \sigma_\alpha$ . When an electric field  $\mathbf{E}$  is applied to the system, the transverse component of the change of magnetization at position  $\mathbf{r}$ , i.e.,  $m(\mathbf{r})\delta\hat{\mathbf{M}}(\mathbf{r})$ , is described by the integral equation

$$m(\mathbf{r})\delta\hat{\mathbf{M}}(\mathbf{r}) = \Xi^{\text{KS}}(\hat{\mathbf{M}}, \mathbf{r})\mathbf{E} + \frac{1}{\mu_0} \int d^3r' \times \chi^{\text{KS}}(\hat{\mathbf{M}}, \mathbf{r}, \mathbf{r}')\Omega^{\text{xc}}(\mathbf{r}')\delta\hat{\mathbf{M}}(\mathbf{r}'). \quad (35)$$

The second term on the right-hand side takes into account that within LSDA the quasiparticles respond not only to the applied fields but also to the induced fields. In order to solve this integral equation approximatively, we assume that the change of magnetization direction is independent of position, i.e.,  $\delta\hat{\mathbf{M}}(\mathbf{r}) = \delta\hat{\mathbf{M}}$ . Multiplying both sides of Eq. (35) by  $\Omega^{\text{xc}}(\mathbf{r})\hat{\mathbf{M}} \times$  from the left, and integrating over position  $\mathbf{r}$  we obtain

$$\bar{\Omega}^{\text{xc}} MV(\hat{\mathbf{M}} \times \delta\hat{\mathbf{M}}) = \mathbf{t}(\hat{\mathbf{M}})\mathbf{E} - \frac{1}{\hbar} \sum_{\alpha\beta} \hat{\mathbf{e}}_\alpha G_{T_\alpha T_\beta}^{\text{R}}(\hbar\omega = 0, \hat{\mathbf{M}})[\hat{\mathbf{M}} \times \delta\hat{\mathbf{M}}]_\beta. \quad (36)$$

The average exchange field on the left-hand side is defined as

$$\bar{\Omega}^{\text{xc}} = \frac{\int d^3r \Omega^{\text{xc}}(\mathbf{r})m(\mathbf{r})}{\int d^3r' m(\mathbf{r}')} = \frac{\int d^3r \Omega^{\text{xc}}(\mathbf{r})m(\mathbf{r})}{MV}. \quad (37)$$

To obtain the first term on the right-hand side of Eq. (36), we made use of

$$\hat{\mathbf{M}} \times \int d^3r \Xi^{\text{KS}}(\hat{\mathbf{M}}, \mathbf{r})\Omega^{\text{xc}}(\mathbf{r}) = \mathbf{t}, \quad (38)$$

which follows from comparison of Eqs. (8) and (33). Solving Eq. (36) for  $\delta\hat{\mathbf{M}}$  and comparing to Eq. (24) yields the following expression for  $\Xi(\hat{\mathbf{M}})$ :

$$\Xi(\hat{\mathbf{M}}) = -\hat{\mathbf{M}} \times \left[ \bar{\Omega}^{\text{xc}} + \frac{G_{T\mathcal{T}}^{\text{R}}(\hbar\omega = 0, \hat{\mathbf{M}})}{MV\hbar} \right]^{-1} \mathbf{t}(\hat{\mathbf{M}}). \quad (39)$$

In order to obtain an expression for  $\chi(\hat{\mathbf{M}})$  in Eq. (28), we need to replace  $\Xi^{\text{KS}}(\hat{\mathbf{M}}, \mathbf{r})\mathbf{E}$  in Eq. (35) by  $\int d^3r' \chi^{\text{KS}}(\hat{\mathbf{M}}, \mathbf{r}, \mathbf{r}')\mathbf{H}^{\text{SOT}}$ , which yields the equation

$$m(\mathbf{r})\delta\hat{\mathbf{M}}(\mathbf{r}) = \int d^3r' \chi^{\text{KS}}(\hat{\mathbf{M}}, \mathbf{r}, \mathbf{r}')\Omega^{\text{xc}}(\mathbf{r}')\frac{\mathbf{H}^{\text{SOT}}}{\bar{\Omega}^{\text{xc}}} + \frac{1}{\mu_0} \int d^3r' \chi^{\text{KS}}(\hat{\mathbf{M}}, \mathbf{r}, \mathbf{r}')\Omega^{\text{xc}}(\mathbf{r}')\delta\hat{\mathbf{M}}(\mathbf{r}'), \quad (40)$$

where we replaced the magnetic field  $\mathbf{H}^{\text{SOT}}$  by  $\mathbf{H}^{\text{SOT}}\Omega^{\text{xc}}(\mathbf{r}')/\bar{\Omega}^{\text{xc}}$  because both magnetic fields produce the same torque on the magnetization [50]:

$$\frac{\mu_0 \hat{\mathbf{M}} \times \mathbf{H}^{\text{SOT}}}{\bar{\Omega}^{\text{xc}}} \int d^3r m(\mathbf{r})\Omega^{\text{xc}}(\mathbf{r}) = \mu_0 V \mathbf{M} \times \mathbf{H}^{\text{SOT}}. \quad (41)$$

Multiplying both sides of Eq. (40) by  $\Omega^{\text{xc}}(\mathbf{r})\hat{\mathbf{M}} \times$  from the left, and integrating over position  $\mathbf{r}$ , we obtain

$$\begin{aligned} & \bar{\Omega}^{\text{xc}} MV(\hat{\mathbf{M}} \times \delta\hat{\mathbf{M}}) \\ &= -\frac{\mu_0}{\hbar \bar{\Omega}^{\text{xc}}} \sum_{\alpha\beta} \hat{\mathbf{e}}_\alpha G_{T_\alpha T_\beta}^{\text{R}}(\hbar\omega = 0, \hat{\mathbf{M}})[\hat{\mathbf{M}} \times \mathbf{H}^{\text{SOT}}]_\beta \\ & \quad - \frac{1}{\hbar} \sum_{\alpha\beta} \hat{\mathbf{e}}_\alpha G_{T_\alpha T_\beta}^{\text{R}}(\hbar\omega = 0, \hat{\mathbf{M}})[\hat{\mathbf{M}} \times \delta\hat{\mathbf{M}}]_\beta. \end{aligned} \quad (42)$$

Comparing Eqs. (42) and (36) leads to

$$\mathbf{t}(\hat{\mathbf{M}})\mathbf{E} = -\frac{\mu_0}{\hbar \bar{\Omega}^{\text{xc}}} G_{T\mathcal{T}}^{\text{R}}(\hbar\omega = 0, \hat{\mathbf{M}})[\hat{\mathbf{M}} \times \mathbf{H}^{\text{SOT}}]. \quad (43)$$

In the absence of SOI,  $G_{T\mathcal{T}}^{\text{R}}(\hbar\omega = 0, \hat{\mathbf{M}})$  is given by (see Appendix)

$$G_{T\mathcal{T}}^{\text{R}}(\hbar\omega = 0, \hat{\mathbf{M}}) = -\hbar MV \bar{\Omega}^{\text{xc}}[1 - \hat{\mathbf{M}}^T \hat{\mathbf{M}}]. \quad (44)$$

We assume that the magnetic anisotropy is small compared to the exchange splitting. In this case, we can approximate  $G_{T\mathcal{T}}^{\text{R}}(\hbar\omega = 0, \hat{\mathbf{M}})$  in Eq. (43) by Eq. (44) and obtain

$$\mathbf{T}^{\text{SOT}} = \mu_0 MV[\hat{\mathbf{M}} \times \mathbf{H}^{\text{SOT}}] = \mathbf{t}(\hat{\mathbf{M}})\mathbf{E}. \quad (45)$$

Equation (45) shows that the description of the SOT through Eq. (32) in terms of many-electron response functions (25) and (29) recovers the single-particle expression (8).

Solving Eq. (42) for  $\delta\hat{\mathbf{M}}$  and comparing to Eq. (28) yields

$$\begin{aligned} \chi(\hat{\mathbf{M}}) &= \frac{\mu_0}{\hbar V \bar{\Omega}^{\text{xc}}} \hat{\mathbf{M}} \times \left[ \bar{\Omega}^{\text{xc}} \right. \\ & \quad \left. + \frac{G_{T\mathcal{T}}^{\text{R}}(\hbar\omega = 0, \hat{\mathbf{M}})}{MV\hbar} \right]^{-1} G_{T\mathcal{T}}^{\text{R}}(\hbar\omega = 0, \hat{\mathbf{M}}) \hat{\mathbf{M}} \times, \end{aligned} \quad (46)$$

where  $\hat{\mathbf{M}} \times$  is a shorthand for the matrix

$$\frac{1}{M} \begin{pmatrix} 0 & -M_3 & M_2 \\ M_3 & 0 & -M_1 \\ -M_2 & M_1 & 0 \end{pmatrix} = \hat{\mathbf{M}} \times. \quad (47)$$

Assuming that the anisotropy energy is much smaller than the exchange splitting, we can approximate the rightmost  $G_{T\mathcal{T}}^{\text{R}}$  in Eq. (46) by Eq. (44) and obtain

$$\chi(\hat{\mathbf{M}}) = -\mu_0 M \hat{\mathbf{M}} \times \left[ \bar{\Omega}^{\text{xc}} + \frac{G_{T\mathcal{T}}^{\text{R}}(\hbar\omega = 0, \hat{\mathbf{M}})}{MV\hbar} \right]^{-1} \hat{\mathbf{M}} \times. \quad (48)$$

The difference between the right-hand and the left-hand sides of Eq. (44) describes the magnetic anisotropy (see Appendix). Therefore, the remaining  $G_{T\mathcal{T}}^{\text{R}}$  in Eq. (48) cannot be approximated by Eq. (44). Inserting Eqs. (48) and (39) into Eq. (32) leads to the identity  $\tilde{\mathbf{t}}(\hat{\mathbf{M}}) = \mathbf{t}(\hat{\mathbf{M}})$ , showing again the equivalence between the single-particle and the many-electron expressions [Eqs. (8) and (32)], respectively.

Using Eq. (48) we can rewrite Eq. (39) as

$$\Xi(\hat{\mathbf{M}}) = -\frac{1}{\mu_0 M} \chi(\hat{\mathbf{M}}) \hat{\mathbf{M}} \times \mathbf{t}(\hat{\mathbf{M}}). \quad (49)$$

In this expression,  $\hat{\mathbf{M}} \times \mathbf{t}(\hat{\mathbf{M}})$  on the right-hand side can be interpreted in terms of a current-induced effective magnetic field  $\mathbf{H}^{\text{SOT}} = -[\hat{\mathbf{M}} \times \mathbf{t}(\hat{\mathbf{M}})\mathbf{E}]/(MV\mu_0)$ . The transverse magnetic susceptibility  $\chi(\hat{\mathbf{M}})$  describes the response of the magnetization to  $\mathbf{H}^{\text{SOT}}$ .

Next, we consider the generation of a current density  $\mathbf{j}$  due to a time-dependent applied magnetic field  $\mathbf{H}^{\text{ext}}(\omega, t) = \mathbf{H}^{\text{ext}}(\omega)e^{-i\omega t}$ . Denoting the corresponding linear-response tensor by  $\Phi(\hat{\mathbf{M}}, \omega)$  we can write

$$\begin{aligned} \mathbf{j} &= \Phi(\hat{\mathbf{M}}, \omega) \mathbf{H}^{\text{ext}}(\omega) e^{-i\omega t} \\ &\simeq \left. \frac{d\Phi(\hat{\mathbf{M}}, \omega)}{d\omega} \right|_{\omega=0} \omega \mathbf{H}^{\text{ext}}(\omega) e^{-i\omega t} \\ &= i\Phi'(\hat{\mathbf{M}}) \frac{d\mathbf{H}^{\text{ext}}(\omega, t)}{d\omega}, \end{aligned} \quad (50)$$

where  $\Phi'(\hat{\mathbf{M}})$  denotes the frequency derivative, i.e.,  $\Phi'(\hat{\mathbf{M}}) = \left. \frac{d\Phi(\hat{\mathbf{M}}, \omega)}{d\omega} \right|_{\omega=0}$ . We used that  $\Phi(\hat{\mathbf{M}}, \omega = 0)$  does not generate an ISOT current and we expanded  $\Phi(\hat{\mathbf{M}}, \omega)$  up to first order in frequency. Assuming that the field  $\mathbf{H}^{\text{ext}}(\omega, t)$  is transverse to magnetization, we can use the transverse magnetic susceptibility  $\chi(\hat{\mathbf{M}})$  [Eq. (28)] to express it in terms of the corresponding tilt of the magnetization direction. This allows us to relate  $\mathbf{j}$  to the time derivative of the magnetization direction:

$$\begin{aligned} \mathbf{j} &= iM\Phi'(\hat{\mathbf{M}})[\chi(\hat{\mathbf{M}})]^{-1} \frac{d\hat{\mathbf{M}}}{dt} \\ &= -iM\Phi'(\hat{\mathbf{M}})[\chi(\hat{\mathbf{M}})]^{-1} \hat{\mathbf{M}} \times \left[ \hat{\mathbf{M}} \times \frac{d\hat{\mathbf{M}}}{dt} \right]. \end{aligned} \quad (51)$$

We can use the retarded velocity spin-moment correlation function

$$\mathcal{G}_{v_\alpha, m_\beta}^R(\hbar\omega, \hat{\mathbf{M}}) = -i \int_0^\infty dt e^{i\omega t} \langle [v_\alpha(t), m_\beta(0)]_- \rangle \quad (52)$$

to express  $\Phi'(\hat{\mathbf{M}})$  as follows:

$$\Phi'_{\alpha\beta}(\hat{\mathbf{M}}) = \lim_{\omega \rightarrow 0} \frac{d}{d\omega} \frac{e\mu_0}{\hbar V} \mathcal{G}_{v_\alpha, m_\beta}^R(\hbar\omega, \hat{\mathbf{M}}). \quad (53)$$

The spectral densities of the Green functions defined in Eqs. (26) and (52) are given by

$$\begin{aligned} S_{m_\alpha, v_\beta}(t, t', \hat{\mathbf{M}}) &= \frac{1}{2\pi} \langle [m_\alpha(t), v_\beta(t')]_- \rangle, \\ S_{v_\alpha, m_\beta}(t, t', \hat{\mathbf{M}}) &= \frac{1}{2\pi} \langle [v_\alpha(t), m_\beta(t')]_- \rangle \end{aligned} \quad (54)$$

and their Fourier transforms satisfy the relations

$$\begin{aligned} S_{m_\alpha, v_\beta}(\hbar\omega, \hat{\mathbf{M}}) &= [S_{v_\beta, m_\alpha}(\hbar\omega, \hat{\mathbf{M}})]^*, \\ \text{Re}[S_{v_\beta, m_\alpha}(\hbar\omega, -\hat{\mathbf{M}})] &= \text{Re}[S_{v_\beta, m_\alpha}(\hbar\omega, \hat{\mathbf{M}})], \\ \text{Im}[S_{v_\beta, m_\alpha}(\hbar\omega, -\hat{\mathbf{M}})] &= -\text{Im}[S_{v_\beta, m_\alpha}(\hbar\omega, \hat{\mathbf{M}})], \end{aligned} \quad (55)$$

from which follows

$$S_{m_\alpha, v_\beta}(\hbar\omega, \hat{\mathbf{M}}) = S_{v_\beta, m_\alpha}(\hbar\omega, -\hat{\mathbf{M}}) \quad (56)$$

and thus

$$\mathcal{G}_{m_\alpha, v_\beta}^R(\hbar\omega, \hat{\mathbf{M}}) = \mathcal{G}_{v_\beta, m_\alpha}^R(\hbar\omega, -\hat{\mathbf{M}}) \quad (57)$$

and

$$\Phi'(\hat{\mathbf{M}}) = \lim_{\omega \rightarrow 0} \frac{d}{d\omega} \frac{e\mu_0}{\hbar V} [\mathcal{G}_{m, v}^R(\hbar\omega, -\hat{\mathbf{M}})]^T. \quad (58)$$

Using Eq. (32),  $[\hat{\mathbf{M}} \times]^T = -\hat{\mathbf{M}} \times$  [see Eq. (47)] and the Onsager relation  $\chi(\hat{\mathbf{M}}) = [\chi(-\hat{\mathbf{M}})]^T$  we can relate  $\Phi'(\hat{\mathbf{M}})$  and the torkance  $\tilde{\mathbf{t}}(\hat{\mathbf{M}})$  as follows:

$$[\tilde{\mathbf{t}}(-\hat{\mathbf{M}})]^T = -iVM\Phi'(\hat{\mathbf{M}})[\chi(\hat{\mathbf{M}})]^{-1} \hat{\mathbf{M}} \times. \quad (59)$$

This allows us to rewrite Eq. (51) as

$$\mathbf{j} = \frac{1}{V} [\tilde{\mathbf{t}}(-\hat{\mathbf{M}})]^T \hat{\mathbf{M}} \times \frac{d\hat{\mathbf{M}}}{dt} \quad (60)$$

in agreement with Eq. (14) derived earlier in the single-particle formalism.

The central result of this section is Eq. (32), which provides a general definition of the torkance that is not limited to the framework of Kohn-Sham theory. The reciprocity between direct and inverse SOT as discussed in the previous subsection based on Kohn-Sham theory remains valid within the many-electron response function formalism used in this section.

### III. SOT AND ISOT IN BILAYER SYSTEMS

In the following, we discuss SOT and ISOT in magnetic bilayer systems composed of a ferromagnetic layer (FM) deposited on a normal metal (NM). When the electric field  $\mathbf{E} = E_x \hat{\mathbf{e}}_x$  is applied in plane along the  $x$  direction, the torques satisfy

$$\begin{aligned} \mathbf{T}^{\text{even}}(\hat{\mathbf{M}}) &= E_x \hat{\mathbf{M}} \times (\hat{\mathbf{e}}_y \times \hat{\mathbf{M}}) [A_0 + A_2(\hat{\mathbf{e}}_z \times \hat{\mathbf{M}})^2 + \dots] \\ &\quad + E_x (\hat{\mathbf{M}} \times \hat{\mathbf{e}}_z)(\hat{\mathbf{M}} \cdot \hat{\mathbf{e}}_x) [B_2 + B_4(\hat{\mathbf{e}}_z \times \hat{\mathbf{M}})^2 + \dots] \end{aligned} \quad (61)$$

and

$$\begin{aligned} \mathbf{T}^{\text{odd}}(\hat{\mathbf{M}}) &= E_x (\hat{\mathbf{e}}_y \times \hat{\mathbf{M}}) [C_0 + C_2(\hat{\mathbf{e}}_z \times \hat{\mathbf{M}})^2 + \dots] \\ &\quad + E_x \hat{\mathbf{M}} \times (\hat{\mathbf{M}} \times \hat{\mathbf{e}}_z)(\hat{\mathbf{M}} \cdot \hat{\mathbf{e}}_x) \\ &\quad \times [D_2 + D_4(\hat{\mathbf{e}}_z \times \hat{\mathbf{M}})^2 + \dots] \end{aligned} \quad (62)$$

in bilayer systems composed of polycrystalline, disordered, or amorphous layers with continuous rotational symmetry around the  $z$  axis [24].

To describe the ISOT in bilayer systems, we consider instead of the current density  $j_\alpha$  the current per length  $J_\alpha$ , which is obtained by replacing the current density operator  $-ev_\alpha/V$  by  $-ev_\alpha/A$ , where  $A$  is the cross-sectional area of the unit cell of the bilayer normal to the stacking direction:

$$J_\alpha(t) = \frac{1}{A} \sum_\beta t_{\beta\alpha}(-\hat{\mathbf{M}}(t)) \left( \hat{\mathbf{M}}(t) \times \frac{d\hat{\mathbf{M}}(t)}{dt} \right)_\beta. \quad (63)$$

Since the atom-resolved current is expected to vary significantly between atomic layers in bilayer systems,  $J_\alpha$  is a suitable definition of current density in such systems. In terms of  $\mathbf{J}$ , the electric current flowing in the  $x$  direction is given by  $I_x = J_x L_y$ , where  $L_y$  is the length of the system in the  $y$  direction, and similarly  $I_y = J_y L_x$  is the electric current in the  $y$  direction. Separating  $J_\alpha$  into the components due to  $\mathbf{t}^{\text{even}}(\hat{\mathbf{M}})$

and  $\mathbf{t}^{\text{odd}}(\hat{\mathbf{M}})$  yields

$$J_{\alpha}^{\text{even}}(t) = \frac{1}{A} \sum_{\beta} t_{\beta\alpha}^{\text{even}}(\hat{\mathbf{M}}(t)) \left( \hat{\mathbf{M}}(t) \times \frac{d\hat{\mathbf{M}}(t)}{dt} \right)_{\beta}, \quad J_{\alpha}^{\text{odd}}(t) = -\frac{1}{A} \sum_{\beta} t_{\beta\alpha}^{\text{odd}}(\hat{\mathbf{M}}(t)) \left( \hat{\mathbf{M}}(t) \times \frac{d\hat{\mathbf{M}}(t)}{dt} \right)_{\beta}. \quad (64)$$

In the following, we discuss the magnetization-dynamics-induced current density  $J_x$  in the  $x$  direction. Using Eqs. (61) and (62) in (64) we obtain

$$J_x^{\text{even}}(t) = \frac{A_0}{A} [\hat{\mathbf{M}} \times (\hat{\mathbf{e}}_y \times \hat{\mathbf{M}})] \cdot \left[ \hat{\mathbf{M}} \times \frac{d\hat{\mathbf{M}}}{dt} \right] + \frac{A_2}{A} [\hat{\mathbf{M}} \times (\hat{\mathbf{e}}_y \times \hat{\mathbf{M}})] \cdot \left[ \hat{\mathbf{M}} \times \frac{d\hat{\mathbf{M}}}{dt} \right] (\hat{\mathbf{e}}_z \times \hat{\mathbf{M}})^2 \\ + \frac{B_2}{A} (\hat{\mathbf{M}} \times \hat{\mathbf{e}}_z) \cdot \left[ \hat{\mathbf{M}} \times \frac{d\hat{\mathbf{M}}}{dt} \right] (\hat{\mathbf{M}} \cdot \hat{\mathbf{e}}_x) + \frac{B_4}{A} (\hat{\mathbf{M}} \times \hat{\mathbf{e}}_z) \cdot \left[ \hat{\mathbf{M}} \times \frac{d\hat{\mathbf{M}}}{dt} \right] (\hat{\mathbf{M}} \cdot \hat{\mathbf{e}}_x) (\hat{\mathbf{e}}_z \times \hat{\mathbf{M}})^2 + \dots \quad (65)$$

and

$$J_x^{\text{odd}}(t) = -\frac{C_0}{A} (\hat{\mathbf{e}}_y \times \hat{\mathbf{M}}) \cdot \left[ \hat{\mathbf{M}} \times \frac{d\hat{\mathbf{M}}}{dt} \right] - \frac{C_2}{A} (\hat{\mathbf{e}}_y \times \hat{\mathbf{M}}) \cdot \left[ \hat{\mathbf{M}} \times \frac{d\hat{\mathbf{M}}}{dt} \right] (\hat{\mathbf{e}}_z \times \hat{\mathbf{M}})^2 \\ - \frac{D_2}{A} [\hat{\mathbf{M}} \times (\hat{\mathbf{M}} \times \hat{\mathbf{e}}_z)] \cdot \left[ \hat{\mathbf{M}} \times \frac{d\hat{\mathbf{M}}}{dt} \right] (\hat{\mathbf{M}} \cdot \hat{\mathbf{e}}_x) - \frac{D_4}{A} [\hat{\mathbf{M}} \times (\hat{\mathbf{M}} \times \hat{\mathbf{e}}_z)] \cdot \left[ \hat{\mathbf{M}} \times \frac{d\hat{\mathbf{M}}}{dt} \right] (\hat{\mathbf{M}} \cdot \hat{\mathbf{e}}_x) (\hat{\mathbf{e}}_z \times \hat{\mathbf{M}})^2 - \dots \quad (66)$$

#### A. Current densities induced by FMR through the inverse SOT

First, we consider the case of FMR-driven magnetization precession around the  $z$  axis in a circular orbit, i.e.,

$$\hat{\mathbf{M}}(t) = [\sin(\theta) \cos(\omega t), \sin(\theta) \sin(\omega t), \cos(\theta)]^T, \quad (67)$$

where  $\theta$  is the cone angle. Inserting Eq. (67) into Eqs. (65) and (66), we obtain

$$J_x^{\text{even}}(t) = -\frac{\omega}{A} \sin(\theta) \cos(\theta) \sin(\omega t) [A_0 + A_2 \sin^2(\theta) + \dots], \\ J_x^{\text{odd}}(t) = \frac{\omega}{A} \sin(\theta) \cos(\omega t) [C_0 + C_2 \sin^2(\theta) + \dots] \\ + \frac{\omega}{A} \sin(\theta) \cos(\omega t) [D_2 \sin^2(\theta) + D_4 \sin^4(\theta) + \dots]. \quad (68)$$

For small-cone angles  $\theta$  the  $\sin^2(\theta)$  factors suppress the contributions from  $A_2$ ,  $C_2$ ,  $D_2$  and further higher-order terms. In the small-cone limit, the ISOT for magnetization precession around the  $z$  axis can thus be expressed in terms of the torkance

for magnetization along  $z$ , if  $A_0 = t_{yx}^{\text{even}}(\hat{\mathbf{M}} = \hat{\mathbf{e}}_z)$  and  $C_0 = t_{xx}^{\text{odd}}(\hat{\mathbf{M}} = \hat{\mathbf{e}}_z)$  are used. Experiments [24,25] and *ab initio* calculations [31] have found that  $A_0$  and  $C_0$  can be of the same order of magnitude in  $\text{AlO}_x/\text{Co}/\text{Pt}$  and  $\text{MgO}/\text{CoFeB}/\text{Ta}$ . The two contributions  $J_x^{\text{even}}(t)$  and  $J_x^{\text{odd}}(t)$  are therefore expected to exhibit similar amplitudes. Since  $J_x^{\text{even}}(t) \propto \sin(\omega t)$  while  $J_x^{\text{odd}}(t) \propto \cos(\omega t)$ , the even and odd parts are phase shifted with respect to each other.

Next, we consider FMR-driven magnetization precession around the  $y$  axis. In this case, the magnetization follows an elliptical trajectory in thin bilayer films due to the demagnetizing field [51]

$$\hat{\mathbf{M}}(t) = \frac{1}{\eta(t)} [\sin(\theta) \sin(\omega t) \epsilon, \cos(\theta), \sin(\theta) \cos(\omega t)]^T, \quad (69)$$

where  $\epsilon$  is the ratio of the major axis to the minor axis of the ellipse and normalization of  $\hat{\mathbf{M}}(t)$  is assured by  $\eta(t) = \sqrt{1 + [\epsilon^2 - 1] \sin^2(\omega t) \sin^2(\theta)}$ . The resulting induced current density is given by

$$J_x^{\text{even}}(t) = \frac{\omega \epsilon \sin^2 \theta}{A \eta^2(t)} \left[ A_0 + A_2 \frac{\eta^2(t) - \cos^2(\omega t) \sin^2 \theta}{\eta^2(t)} + \dots \right] - \frac{\omega \epsilon \sin^2 \theta \sin^2(\omega t)}{A \eta^4(t)} [1 + \sin^2 \theta (\epsilon^2 - 1)] \\ \times \left[ B_2 + B_4 \frac{\eta^2(t) - \cos^2(\omega t) \sin^2 \theta}{\eta^2(t)} + \dots \right], \quad (70) \\ J_x^{\text{odd}}(t) = \frac{\omega(1 - \epsilon^2)}{2A \eta^3(t)} \sin^2 \theta \cos \theta \sin(2\omega t) \left[ C_0 + C_2 \frac{\eta^2(t) - \cos^2(\omega t) \sin^2 \theta}{\eta^2(t)} + \dots \right] \\ - \frac{\omega \epsilon^2}{2A \eta^3(t)} \sin(2\omega t) \sin^2 \theta \cos \theta \left[ D_2 + D_4 \frac{\eta^2(t) - \cos^2(\omega t) \sin^2 \theta}{\eta^2(t)} + \dots \right].$$

For small angles  $\theta$  the terms proportional to  $\sin^2 \theta$  dominate, while terms proportional to  $\sin^4 \theta$  and higher are suppressed. Thus, we can approximate in the small-cone limit

$$J_x^{\text{even}}(t) = \frac{\omega \epsilon}{A} \sin^2 \theta [A_0 + A_2 + A_4 + \dots] - \frac{\omega \epsilon}{2A} \sin^2 \theta [1 - \cos(2\omega t)] [B_2 + B_4 + \dots], \quad (71) \\ J_x^{\text{odd}}(t) = \frac{\omega}{2A} \sin^2 \theta \sin(2\omega t) (1 - \epsilon^2) [C_0 + C_2 + \dots] - \frac{\omega}{2A} \sin^2 \theta \sin(2\omega t) \epsilon^2 [D_2 + D_4 + \dots].$$

$J_x^{\text{even}}$  is the sum of a dc component and an ac component with frequency  $2\omega$ , while  $J_x^{\text{odd}}$  consists of only an ac part with frequency  $2\omega$ . The ac components of the even and odd parts are phase shifted. Compared to the induced current for precession around the  $z$  axis [Eq. (68)], the amplitude is expected to be typically reduced by roughly a factor of  $\sin\theta$  when the magnetization precesses around the  $y$  axis. The dc component of the voltage  $-R_{xx}J_x^{\text{even}}L_y$ , where  $R_{xx}$  is the resistance, has been measured for several bilayer systems and is usually interpreted as the voltage arising from the conversion of pumped dc spin current via the ISHE [34–36].

We turn now to the FMR-driven magnetization precession around the  $x$  axis. Again, the magnetization follows an elliptical trajectory

$$\hat{\mathbf{M}}(t) = \frac{1}{\tilde{\eta}(t)} [\cos(\theta), \sin(\theta) \cos(\omega t) \epsilon, \sin(\theta) \sin(\omega t)]^T, \quad (72)$$

with  $\epsilon$  the ratio of major axis to minor axis of the ellipse and  $\tilde{\eta}(t) = \sqrt{1 + [\epsilon^2 - 1] \cos^2(\omega t) \sin^2(\theta)}$ . In this case, the current density induced by the precessing magnetization is given by

$$\begin{aligned} J_x^{\text{even}}(t) &= -\frac{\omega}{2A\tilde{\eta}^2(t)} \sin(2\theta) \cos(\omega t) \left\{ A_0 + \frac{A_2}{\tilde{\eta}^2(t)} [\cos^2\theta + \epsilon^2 \sin^2\theta \cos^2(\omega t)] + \dots \right\} \\ &\quad + \frac{\omega}{2A\tilde{\eta}^4(t)} \sin(2\theta) \cos(\omega t) [1 + \sin^2\theta(\epsilon^2 - 1)] \left\{ B_2 + \frac{B_4}{\tilde{\eta}^2(t)} [\cos^2\theta + \epsilon^2 \sin^2\theta \cos^2(\omega t)] + \dots \right\}, \\ J_x^{\text{odd}}(t) &= -\frac{\omega\epsilon}{A\tilde{\eta}^3(t)} \sin\theta \sin(\omega t) \left\{ C_0 + \frac{C_2}{\tilde{\eta}^2(t)} [\cos^2\theta + \epsilon^2 \sin^2\theta \cos^2(\omega t)] + \dots \right\} \\ &\quad - \frac{\omega\epsilon}{A\tilde{\eta}^3(t)} \sin\theta \cos^2\theta \sin(\omega t) \left\{ D_2 + \frac{D_4}{\tilde{\eta}^2(t)} [\cos^2\theta + \epsilon^2 \sin^2\theta \cos^2(\omega t)] + \dots \right\}. \end{aligned} \quad (73)$$

In the small-cone limit, we obtain

$$\begin{aligned} J_x^{\text{even}}(t) &= \frac{\omega}{2A} \sin(2\theta) \cos(\omega t) [B_2 + B_4 + \dots - A_0 - A_2 - \dots] = -t_{yx}^{\text{even}}(\hat{\mathbf{M}} = \hat{\mathbf{e}}_x) \frac{\omega}{2A} \sin(2\theta) \cos(\omega t), \\ J_x^{\text{odd}}(t) &= -\frac{\omega}{A} \epsilon \sin\theta \sin(\omega t) [C_0 + C_2 + \dots + D_2 + D_4 + \dots] = t_{zx}^{\text{odd}}(\hat{\mathbf{M}} = \hat{\mathbf{e}}_x) \frac{\omega}{A} \epsilon \sin\theta \sin(\omega t). \end{aligned} \quad (74)$$

Even if  $A_2$ ,  $B_2$ ,  $C_2$ , and  $D_2$  are nonzero, i.e., even in the presence of anisotropic SOT, the ISOT for magnetization precession around the  $x$  axis can thus be expressed in terms of the torque for magnetization along  $x$ . The even and odd contributions are again phase shifted and the dependence on the cone angle is  $\propto \sin\theta$  in the limit of small  $\theta$  as in the case of magnetization precession around the  $z$  axis, promising a significantly larger ISOT signal [39] compared to the case with magnetization precession around the  $y$  axis.

The main result of this section are the expressions for the ISOT currents given in Eq. (68) (magnetization precession around  $z$ ), Eq. (71) (magnetization precession around  $y$ ), and Eq. (74) (magnetization precession around  $x$ ). We stress that these expressions have been derived without any assumptions on the underlying mechanism (such as SHE or interfacial SOI) and are thus generally valid in bilayer systems with continuous rotational symmetry around the  $z$  axis. In all three cases, the coefficients  $C_0$ ,  $C_2$ ,  $\dots$  and  $D_2$ ,  $D_4$ ,  $\dots$ , which govern the odd torque, give rise to an ac current, but never to a dc current. Thus, complete characterization of ISOT in experiments requires the measurement of the ac component.

## B. Reciprocity between the even SOT and the even ISOT

In magnetic bilayer systems that involve a normal metal (NM) layer with large SHE it is expected that an important contribution to the even SOT arises from SHE [22,23,27,52]. In particular when the NM layer is thin, the SHE in the NM

layer will generally differ from the SHE in a corresponding bulk system. Even when the NM layer is thick, close to the interface with the magnet the electronic structure is modified due to the hybridization of the electronic states of the NM with those of the ferromagnet (FM). This electronic-structure change is expected to entail a modification of the SHE in the NM close to the interface. Furthermore, the proximity with the FM layer induces magnetic moments in the NM at the interface due to which the SHE is also modified [53]. Additionally, qualitatively new mechanisms for SHE are added by the presence of the interface: When an electric field is applied to the bilayer in the in-plane direction, part of the in-plane electric current is carried by interface states that are evanescent waves along the stacking direction in the NM. That evanescent waves can also contribute to the SHE has been discussed [54] in the context of tunnel junctions but is also true for evanescent waves in all-metallic bilayer systems.

Rather than using the term SHE only for the bulk contribution, we will in this work often denote by SHE the total spin current generated by an applied electric field, including the interface modifications discussed above into the term SHE. Recently, we have shown within *ab initio* calculations that the even SOT in Co/Pt and Mn/W bilayers arises from the flux of spin current from the NM into the FM layer [31]. Within our terminology, this spin flux arises from the SHE.

In the following, we discuss a minimal model to describe the SHE contribution to the even SOT. We consider a bilayer system composed of a semi-infinite ferromagnetic layer (FM)



on a semi-infinite normal metal (NM). The interface between FM and NM is located at  $z = 0$ . We estimate the SOT arising from the SHE in NM, when an electric field  $E_x \hat{e}_x$  is applied in the  $x$  direction. Deep inside NM, i.e., for  $z \ll 0$ , the spin current density flowing in the  $z$  direction is

$$Q_y = \sigma_{zx}^y E_x = \frac{\hbar}{2e} \sigma_{xx} E_x \tan \gamma_{\text{SHE}}, \quad (75)$$

where  $\sigma_{zx}^y$  is the SHE conductivity in NM,  $\tan \gamma_{\text{SHE}}$  is the SHE angle, and  $\sigma_{xx}$  is the normal conductivity in NM. As discussed above, the SHE is generally expected to be modified close to the NM/FM interface. However, in order to obtain a minimal model, we neglect this expected position dependence of SHE and assume that the SHE can effectively be described by a single parameter  $\sigma_{zx}^y$ . We assume that a fraction  $\xi$  of  $Q_y$  is transmitted through the NM/FM interface and absorbed by FM, thereby causing a torque on its magnetization, which we assume to point in the  $z$  direction. This SHE-to-SOT efficiency  $\xi$  can be thought of as the spin-current transmissivity [55] or transparency [56] of the NM/FM interface. In metallic magnetic bilayer systems,  $\xi$  is typically of the order of 1: in experiments on NiFe/Pt, it was estimated to be  $\xi \approx 0.4$ – $0.6$  [55]. In *ab initio* calculations of FePt/Pt,  $\xi \approx 0.6$  was found [57]. Denoting the  $xy$  cross-sectional area of the unit cell by  $A$ , the torque per unit cell is given by  $T_y^{\text{even}} = \xi A Q_y = t_{yx}^{\text{even}} E_x$  with

$$t_{yx}^{\text{even}}(\hat{M} = \hat{e}_z) = \xi A \sigma_{zx}^y = \xi A \frac{\hbar}{2e} \sigma_{xx} \tan \gamma_{\text{SHE}}. \quad (76)$$

Next, we consider the even ISOT arising from the combined action of spin pumping and ISHE. The spin current density pumped adiabatically into NM is determined by [33]

$$Q(z=0) = \frac{\hbar}{4\pi} \text{Reg}^{\uparrow\downarrow} \hat{M} \times \frac{d\hat{M}}{dt}, \quad (77)$$

where  $g^{\uparrow\downarrow}$  is the (generally complex) spin-mixing conductance per cross-sectional area. The imaginary part of  $g^{\uparrow\downarrow}$  is assumed to be negligible in Eq. (77). If spin transport in NM is diffusive, a spin accumulation  $s(z)$  forms in NM due to the spins pumped into NM. The spin current in NM is proportional to the gradient of the spin accumulation  $s(z)$ . Since the spin accumulation decays exponentially in NM,  $s(z) = s(0)e^{z/\lambda_{\text{sd}}}$ , where  $\lambda_{\text{sd}}$  is the spin-diffusion length, also the spin current decays exponentially in NM, i.e.,  $Q(z) = Q(0)e^{z/\lambda_{\text{sd}}}$  [34,39]. In the case of magnetization precession around the  $y$  axis [Eq. (69)], the dc spin current flowing in NM in the  $z$  direction is therefore given by

$$Q_y(z) = -\frac{\hbar\omega}{4\pi} \text{Reg}^{\uparrow\downarrow} \sin^2(\theta) e^{z/\lambda_{\text{sd}}}. \quad (78)$$

Due to ISHE this spin current is converted into an in-plane charge current flowing in the  $x$  direction:

$$\begin{aligned} j_x^{\text{even}}(z) &= -\frac{2e}{\hbar} Q_y(z) \tan \gamma_{\text{ISHE}} \\ &= \frac{e\omega}{2\pi} \text{Reg}^{\uparrow\downarrow} \sin^2(\theta) e^{z/\lambda_{\text{sd}}} \tan \gamma_{\text{ISHE}}, \end{aligned} \quad (79)$$

where  $\tan \gamma_{\text{ISHE}}$  is the ISHE angle. Thus, a single characteristic length, the spin-diffusion length  $\lambda_{\text{sd}}$ , determines the position

dependence of  $s(z)$ ,  $Q_y(z)$ , and  $j_x^{\text{even}}(z)$  within this model:

$$j_x^{\text{even}}(z) \propto Q_y(z) \propto s(z) \propto e^{z/\lambda_{\text{sd}}}. \quad (80)$$

Integration of the current density (79) from  $z = -\infty$  to  $z = 0$  yields the current per length flowing in NM:

$$J_x^{\text{even}} = \frac{e\omega}{2\pi} \text{Reg}^{\uparrow\downarrow} \sin^2(\theta) \epsilon \lambda_{\text{sd}} \tan \gamma_{\text{ISHE}}. \quad (81)$$

Using the small-cone limit of Eq. (70) and assuming  $A_2 = B_2 = A_4 = \dots = 0$ , we obtain the alternative expression

$$J_x^{\text{even}} = \frac{\omega}{A} \sin^2(\theta) \epsilon A_0. \quad (82)$$

Equating the two expressions for  $J_x^{\text{even}}$  yields

$$A_0 = A \frac{e}{2\pi} \text{Reg}^{\uparrow\downarrow} \lambda_{\text{sd}} \tan \gamma_{\text{ISHE}}. \quad (83)$$

Application of  $t_{yx}^{\text{even}}(\hat{M} = \hat{e}_z) = A_0$  leads to

$$\lambda_{\text{sd}} = \frac{2\pi t_{yx}^{\text{even}}(\hat{M} = \hat{e}_z)}{e A \text{Reg}^{\uparrow\downarrow} \tan \gamma_{\text{ISHE}}}. \quad (84)$$

Employing Eq. (76) and assuming  $\tan \gamma_{\text{ISHE}} = \tan \gamma_{\text{SHE}}$  we can recast Eq. (84) as

$$\lambda_{\text{sd}} = \frac{\xi \hbar \pi \sigma_{xx}}{e^2 \text{Reg}^{\uparrow\downarrow}}. \quad (85)$$

Equation (85) relates the SHE-to-SOT efficiency  $\xi$  with the parameters we use to model the ISOT current and thereby expresses the reciprocity between SOT and ISOT.

Even though this minimal model is derived for semi-infinite layers, it can be applied to bilayers of finite thickness when the layer thickness is much larger than  $\lambda_{\text{sd}}$ . When NM has the finite thickness  $D$ , i.e.,  $-D \leq z \leq 0$ , and when  $D \gg \lambda_{\text{sd}}$  is not satisfied, Eq. (78) needs to be replaced by [34]

$$Q_y(z) = -\frac{\hbar\omega}{4\pi} \text{Reg}^{\uparrow\downarrow} \sin^2(\theta) \epsilon \frac{\sinh \frac{z+D}{\lambda_{\text{sd}}}}{\sinh \frac{D}{\lambda_{\text{sd}}}} \quad (86)$$

in order to take into account that the spin current is reflected at the boundary of NM at  $z = -D$ .

In Secs. IV B and IV C, we will compare ISOT current and spin-current densities obtained from *ab initio* calculations to the minimal model described above. We will show that the minimal model provides a satisfactory description of the *ab initio* results. We will discuss that the main shortcoming of the minimal model is the assumption that SHE and ISHE can be described by a single position-independent parameter, whereby the modification of SHE and ISHE close to the interface is neglected.

### C. Reciprocity between the odd SOT and the odd ISOT

In Sec. II, we demonstrated the reciprocity between ISOT and SOT on general grounds. The odd SOT in the bilayer systems considered in this work arises dominantly from the intraband contribution to Eq. (8). This intraband contribution can also be obtained from Boltzmann transport theory within the constant relaxation-time approximation. In this section, we study the odd SOT and the odd ISOT within Boltzmann

transport theory and show that the obtained expressions satisfy the reciprocity formulated previously in Sec. II.

When an electric field  $\mathbf{E}$  is applied, the occupation number  $f_{kn}$  of band  $n$  at  $k$  point  $\mathbf{k}$  changes according to

$$\delta f_{kn}^{(1)} = -e\tau \mathbf{v}_{kn} \cdot \mathbf{E} \delta(\mathcal{E}_F - \mathcal{E}_{kn}), \quad (87)$$

where  $\tau$  is the relaxation time,  $\mathcal{E}_F$  is the Fermi energy, and  $\mathbf{v}_{kn} = \langle \psi_{kn} | \mathbf{v} | \psi_{kn} \rangle$  is the group velocity of band  $n$  at  $k$  point  $\mathbf{k}$ . The change  $\delta f_{kn}^{(1)}$  of the occupancies results in the contribution

$$\begin{aligned} j_\alpha^{(1)} &= -\frac{e}{V\mathcal{N}} \sum_{kn} v_{k\alpha n} \delta f_{kn}^{(1)} \\ &= \frac{e^2\tau}{V\mathcal{N}} \sum_{kn\beta} v_{k\alpha n} v_{k\beta n} E_\beta \delta(\mathcal{E}_F - \mathcal{E}_{kn}) \end{aligned} \quad (88)$$

to the electric current density and in the contribution

$$\begin{aligned} T_\alpha^{(1)} &= -\sum_{kn} \mathcal{T}_{k\alpha n} \delta f_{kn}^{(1)} \\ &= \frac{e\tau}{\mathcal{N}} \sum_{kn\beta} \mathcal{T}_{k\alpha n} v_{k\beta n} E_\beta \delta(\mathcal{E}_F - \mathcal{E}_{kn}), \end{aligned} \quad (89)$$

to the torque, where  $v_{k\alpha n}$  and  $\mathcal{T}_{k\alpha n}$  are the  $\alpha$ th Cartesian components of the group velocity  $\mathbf{v}_{kn}$  and of the torque  $\mathcal{T}_{kn} = \langle \psi_{kn} | \mathcal{T} | \psi_{kn} \rangle$ , respectively.

When the system is perturbed not by an electric field but by the time dependence of the magnetization direction  $\hat{\mathbf{M}}(t)$ , the change of the occupancies is given by

$$\delta f_{kn}^{(2)} = \tau \delta(\mathcal{E}_F - \mathcal{E}_{kn}) \mathcal{T}_{kn} \cdot \left[ \hat{\mathbf{M}}(t) \times \frac{d\hat{\mathbf{M}}(t)}{dt} \right] \quad (90)$$

instead of Eq. (87). Equation (90) follows from

$$\begin{aligned} \frac{\delta f_{kn}^{(2)}}{\tau} &= -\frac{\partial f_{kn}}{\partial \hat{\mathbf{M}}} \cdot \frac{d\hat{\mathbf{M}}}{dt} = -\frac{\partial f_{kn}}{\partial \mathcal{E}_{kn}} \frac{\partial \mathcal{E}_{kn}}{\partial \hat{\mathbf{M}}} \cdot \frac{d\hat{\mathbf{M}}}{dt} \\ &= \delta(\mathcal{E}_F - \mathcal{E}_{kn}) \left[ \hat{\mathbf{M}}(t) \times \frac{\partial \mathcal{E}_{kn}}{\partial \hat{\mathbf{M}}} \right] \cdot \left[ \hat{\mathbf{M}}(t) \times \frac{d\hat{\mathbf{M}}(t)}{dt} \right] \\ &= \delta(\mathcal{E}_F - \mathcal{E}_{kn}) \mathcal{T}_{kn} \cdot \left[ \hat{\mathbf{M}}(t) \times \frac{d\hat{\mathbf{M}}(t)}{dt} \right], \end{aligned} \quad (91)$$

where we set the temperature in the Fermi-Dirac distribution function to zero such that  $f_{kn} = \theta(\mathcal{E}_F - \mathcal{E}_{kn})$  and  $\partial f_{kn} / \partial \mathcal{E}_{kn} = -\delta(\mathcal{E}_F - \mathcal{E}_{kn})$ . Additionally, we made use of

$$\left[ \hat{\mathbf{M}}(t) \times \frac{\partial \mathcal{E}_{kn}}{\partial \hat{\mathbf{M}}} \right] = \hat{\mathbf{M}}(t) \times \langle \psi_{kn} | \frac{\partial H_{\hat{\mathbf{M}}}}{\partial \hat{\mathbf{M}}} | \psi_{kn} \rangle = \mathcal{T}_{kn}. \quad (92)$$

Equations (90) and (91) hold under the condition that the frequency  $\omega$  of the precession of magnetization is small compared to the relaxation rate  $\tau^{-1}$ , i.e.,  $\omega \ll \tau^{-1}$ . If the condition  $\omega \ll \tau^{-1}$  is violated, one needs to solve the Boltzmann equation assuming an explicit time dependence of the distribution function. The expressions valid in that case are obtained by replacing  $\tau$  in Eqs. (90) and (91) as follows:

$$\tau \rightarrow \frac{\tau}{1 - i\omega\tau}. \quad (93)$$

For magnetic bilayers such as Co/Pt we estimate that  $10 \text{ THz} < 1/(2\pi\tau)$ , which is much larger than ferromagnetic resonance frequencies in the GHz range. Therefore, we will always assume  $\omega \ll \tau^{-1}$  in the following.

The current density induced due to the time dependence of magnetization can be obtained from the change of occupancies  $\delta f_{kn}^{(2)}$  given in Eq. (90):

$$\begin{aligned} j_\alpha^{(2)} &= -\frac{e}{V\mathcal{N}} \sum_{kn} v_{k\alpha n} \delta f_{kn}^{(2)} \\ &= -\frac{e\tau}{V\mathcal{N}} \sum_{kn} v_{k\alpha n} \delta(\mathcal{E}_F - \mathcal{E}_{kn}) \mathcal{T}_{kn} \cdot \left[ \hat{\mathbf{M}}(t) \times \frac{d\hat{\mathbf{M}}(t)}{dt} \right]. \end{aligned} \quad (94)$$

Similarly, the torque which damps the magnetization dynamics is given by

$$\begin{aligned} T_\alpha^{(2)} &= -\frac{1}{\mathcal{N}} \sum_{kn} \mathcal{T}_{k\alpha n} \delta f_{kn}^{(2)} \\ &= -\frac{\tau}{\mathcal{N}} \sum_{kn} \mathcal{T}_{k\alpha n} \delta(\mathcal{E}_F - \mathcal{E}_{kn}) \mathcal{T}_{kn} \cdot \left[ \hat{\mathbf{M}}(t) \times \frac{d\hat{\mathbf{M}}(t)}{dt} \right]. \end{aligned} \quad (95)$$

We can combine Eqs. (88), (89), (94), and (95) in the form of Eq. (22) as follows:

$$\begin{pmatrix} \tilde{\mathbf{j}} \\ \tilde{\mathbf{T}}/V \end{pmatrix} = \begin{pmatrix} \tilde{\boldsymbol{\sigma}} & -\tilde{\mathbf{t}}^T/V \\ \tilde{\mathbf{t}}/V & -\tilde{\mathbf{\Lambda}} \end{pmatrix} \begin{pmatrix} \mathbf{E} \\ \hat{\mathbf{M}} \times \frac{d\hat{\mathbf{M}}}{dt} \end{pmatrix}, \quad (96)$$

where we defined  $\tilde{\mathbf{j}} = \mathbf{j}^{(1)} + \mathbf{j}^{(2)}$  and  $\tilde{\mathbf{T}} = \mathbf{T}^{(1)} + \mathbf{T}^{(2)}$ . We use the tilde to recall that according to Eqs. (88), (89), (94), and (95), only intraband terms are considered in  $\tilde{\mathbf{j}}$  and  $\tilde{\mathbf{T}}$ , while the complete expression for current density and torque contains additional interband terms. The linear response coefficients  $\tilde{\boldsymbol{\sigma}}$ ,  $\tilde{\mathbf{t}}$ , and  $\tilde{\mathbf{\Lambda}}$  are given by

$$\begin{aligned} \tilde{\sigma}_{\alpha\beta} &= \frac{e^2\tau}{V\mathcal{N}} \sum_{kn} v_{k\alpha n} v_{k\beta n} \delta(\mathcal{E}_F - \mathcal{E}_{kn}), \\ \tilde{t}_{\alpha\beta} &= \frac{e\tau}{\mathcal{N}} \sum_{kn} \mathcal{T}_{k\alpha n} v_{k\beta n} \delta(\mathcal{E}_F - \mathcal{E}_{kn}), \\ \tilde{\Lambda}_{\alpha\beta} &= \frac{\tau}{V\mathcal{N}} \sum_{kn} \mathcal{T}_{k\alpha n} \mathcal{T}_{k\beta n} \delta(\mathcal{E}_F - \mathcal{E}_{kn}). \end{aligned} \quad (97)$$

$\tilde{\boldsymbol{\sigma}}$  and  $\tilde{\mathbf{\Lambda}}$  are even with respect to reversal of magnetization direction  $\hat{\mathbf{M}}$ , while  $\tilde{\mathbf{t}}$  is odd. Equation (96) clearly shows that the tensor  $\tilde{\mathbf{t}}$  governs both the odd SOT and the odd ISOT. The Gilbert damping  $\tilde{\alpha}$  is related to  $\tilde{\mathbf{\Lambda}}$  by  $\tilde{\alpha} = |\gamma| \tilde{\mathbf{\Lambda}} / (\mu_0 M)$  [see Eq. (20)], i.e.,

$$\tilde{\alpha}_{\alpha\beta} = \frac{|\gamma|\tau}{\mu_0 V M \mathcal{N}} \sum_{kn} \mathcal{T}_{k\alpha n} \mathcal{T}_{k\beta n} \delta(\mathcal{E}_F - \mathcal{E}_{kn}), \quad (98)$$

which agrees with the intraband term in the torque-correlation formula of the Gilbert damping [50,58,59]. Thus, Eq. (90) leads to a coherent description of the intraband contributions to both the Gilbert damping and the odd ISOT. Moreover, the expression obtained for the odd ISOT is reciprocal to the odd direct SOT.

#### IV. FIRST-PRINCIPLES CALCULATIONS

##### A. Computational method

In the following, we will discuss SOTs and ISOTs for a bilayer composed of 3 layers of hcp Co on 20 layers of fcc Pt(111), denoted in the following as Co(3)/Pt(20). We label the atomic layers of the Pt layer by Pt1 through Pt20, where Pt20 is at the Co/Pt interface. Likewise, we label the atomic layers of the Co layer by Co1 through Co3, where Co1 is at the Co/Pt interface. We introduce a Cartesian coordinate system such that the  $z$  axis is perpendicular to the atomic layers, i.e., along the out-of-plane direction, and Pt20 has a smaller  $z$  coordinate than Co1. The magnetization direction is set to  $\hat{\mathbf{M}} = \hat{\mathbf{e}}_z$  in the calculation. In order to perform the linear-response calculations of the torkance computationally efficiently, the Wannier interpolation technique is employed [60–62]. For this purpose, we express the electronic structure in terms of maximally localized Wannier functions (MLWFs), using 18 MLWFs per atom. Details of the electronic-structure calculation of Co(3)/Pt(20) are given in Ref. [31].

Within the independent particle approximation, the torkance  $\mathbf{t}$  defined in Eq. (8) can be expressed as sum of three terms  $t_{\alpha\beta} = t_{\alpha\beta}^{I(a)} + t_{\alpha\beta}^{I(b)} + t_{\alpha\beta}^{II}$ , where [31,45]

$$\begin{aligned} t_{\alpha\beta}^{I(a)} &= \frac{e}{\mathcal{N}h} \sum_k \text{Tr} \langle \mathcal{T}_\alpha G_k^R(\mathcal{E}_F) v_\beta G_k^A(\mathcal{E}_F) \rangle, \\ t_{\alpha\beta}^{I(b)} &= -\frac{e}{\mathcal{N}h} \sum_k \text{Re Tr} \langle \mathcal{T}_\alpha G_k^R(\mathcal{E}_F) v_\beta G_k^R(\mathcal{E}_F) \rangle, \\ t_{\alpha\beta}^{II} &= \frac{e}{\mathcal{N}h} \sum_k \int_{-\infty}^{\mathcal{E}_F} d\mathcal{E} \text{Re Tr} \left\langle \mathcal{T}_\alpha G_k^R(\mathcal{E}) v_\beta \frac{dG_k^R(\mathcal{E})}{d\mathcal{E}} \right. \\ &\quad \left. - \mathcal{T}_\alpha \frac{dG_k^R(\mathcal{E})}{d\mathcal{E}} v_\beta G_k^R(\mathcal{E}) \right\rangle, \end{aligned} \quad (99)$$

with  $G_k^R(\mathcal{E})$  the retarded Green function at  $k$  point  $\mathbf{k}$  and energy  $\mathcal{E}$ ,  $G_k^A(\mathcal{E})$  the advanced one,  $\mathcal{N}$  the number of  $k$  points, and  $\mathcal{E}_F$  the Fermi energy. We model the effect of disorder by a phenomenological band broadening  $\Gamma$  in the Green functions, i.e.,  $G_k^R(\mathcal{E}) = \hbar[\mathcal{E} - H_k + i\Gamma]^{-1}$ .

We discuss the direct SOT in terms of the torkance, which we compute according to Eq. (99). In order to obtain atom-resolved torkances, we replace the torque operator in Eq. (99) by an atom-resolved torque operator (see Ref. [31] for details). We calculate the induced ISOT current in the Co(3)/Pt(20) bilayer using Eq. (64) and the torkance obtained from Eq. (99). However, it is desirable to determine also the spatial profile of the ISOT current along the  $z$  direction. For this purpose, we define the layer-resolved velocity operator

$$v_{kanm}(L) = v_{kanm} \theta_n(L) \theta_m(L), \quad (100)$$

where  $\theta_m(L) = 1$  if MLWF orbital  $m$  belongs to layer  $L$  and zero otherwise. Here, each MLWF is attributed to the one atomic layer in which the center of the MLWF is located and

$$v_{kanm} = \frac{1}{\hbar} \sum_{\mathbf{R}} e^{i\mathbf{k} \cdot \mathbf{R}} i R_\alpha \langle W_{n0} | H | W_{m\mathbf{R}} \rangle \quad (101)$$

is the  $\alpha$ th Cartesian component of the velocity operator at  $k$  point  $\mathbf{k}$  expressed in the basis of Wannier functions. Replacing

$v_\alpha$  in Eq. (99) by  $v_\alpha(L)$  allows us to compute the ISOT current within the atomic layer  $L$ .

The direct SOT is a response to the applied electric field  $\mathbf{E}$ , which exerts the mechanical force  $-e\mathbf{E}$  on the electrons. By artificially switching off the force  $-e\mathbf{E}$  for some atomic layers, we investigate which atomic layers participate in generating the SOT. Noting that the mechanical force is represented in Eq. (99) by the velocity operator, we replace  $v_\alpha$  in Eq. (99) by  $v_\alpha(L)$  in order to study the SOT generated when the force  $-e\mathbf{E}$  acts only on the electrons in the atomic layer  $L$ . Thus, the replacement of  $v_\alpha$  by  $v_\alpha(L)$  in Eq. (99) provides us not only with the information on how the ISOT current is distributed in Co(3)/Pt(20) along the stacking direction, but additionally it also provides us with the information in which atomic layers action of the force  $-e\mathbf{E}$  is essential for the direct SOT. This results from the reciprocity between ISOT and SOT, which implies that the atomic layers that carry the ISOT current agree to the atomic layers that participate in generating the SOT. In order to describe the situation where the mechanical force is switched off for the atomic layers Pt1 through  $L-1$  we use the sum of Eq. (100) for the layers  $L, L+1, \dots$ , i.e., we use the modified velocity operator

$$\bar{v}_{kanm}(L) = v_{kanm} \sum_{L_1 \geq L} \sum_{L_2 \geq L} \theta_n(L_1) \theta_m(L_2) \quad (102)$$

in Eq. (99). Here, the functions  $\theta_m(L)$  are defined as above, below Eq. (100).

As discussed in Sec. III B, the spin current flowing in the  $z$  direction mediates an important contribution to the even ISOT in bilayer systems. Thus, it is desirable to determine its spatial profile along the  $z$  direction. For this purpose, we define the layer-resolved spin-current density operator  $\mathcal{Q}_s(L)$  for spin currents flowing in the  $z$  direction by

$$\langle \psi_{kn} | \mathcal{Q}_s(L) | \psi_{km} \rangle = \frac{1}{A} \int_{S_L} d\mathbf{S} \cdot \langle \psi_{kn} | \mathcal{Q}_s(\mathbf{r}) | \psi_{km} \rangle, \quad (103)$$

where the integration is over the boundary  $S_L$  between layers  $L-1$  and  $L$ ,  $A$  is the  $xy$  cross-sectional area of the unit cell, and  $\mathcal{Q}_s(\mathbf{r})$  is the spin-current density operator at point  $\mathbf{r}$ . SOI is only strong close to the atomic nuclei because it is proportional to the electrostatic potential gradient. Since the boundary  $S_L$  is chosen to lie in the interstitial region, where SOI is negligible, the nonrelativistic spin-current density operator can be used:

$$\mathcal{Q}_s(\mathbf{r}) = \frac{\hbar}{2} \frac{\hbar}{2im} [\delta(\mathbf{r} - \hat{\mathbf{r}}) \vec{\nabla} - \overleftarrow{\nabla} \delta(\mathbf{r} - \hat{\mathbf{r}})] \sigma_s. \quad (104)$$

By replacing in Eq. (5) the current density operator  $-ev_\alpha/V$  by  $\mathcal{Q}_s(L)$ , we can determine the spin-current profile along the stacking direction of the Co(3)/Pt(20) bilayer:

$$\mathcal{Q}_s(L, t) = \frac{1}{A} \sum_{\beta} w_{s\beta}(L, \hat{\mathbf{M}}(t)) \left[ \hat{\mathbf{M}}(t) \times \frac{d\hat{\mathbf{M}}(t)}{dt} \right]_{\beta}, \quad (105)$$

where we defined

$$w_{s\beta}(L, \hat{\mathbf{M}}) = -A \lim_{\omega \rightarrow 0} \frac{\text{Im} G_{\mathcal{Q}_s(L), T_\beta}^R(\hbar\omega, \hat{\mathbf{M}})}{\hbar\omega}, \quad (106)$$

with the Fourier transform of the retarded spin-current torque correlation function

$$G_{Q_s(L), T_\beta}^R(\hbar\omega, \hat{M}) = -i \int_0^\infty dt e^{i\omega t} \langle [Q_s(L), T_\beta(-t)]_- \rangle. \quad (107)$$

Within the independent particle approximation Eq. (106) becomes  $w_{s\beta}(L) = w_{s\beta}^{I(a)}(L) + w_{s\beta}^{I(b)}(L) + w_{s\beta}^{II}(L)$ , with

$$\begin{aligned} w_{s\beta}^{I(a)}(L) &= \frac{eA}{N\hbar} \sum_k \text{Tr} \langle Q_s(L) G_k^R(\mathcal{E}_F) T_\beta G_k^A(\mathcal{E}_F) \rangle, \\ w_{s\beta}^{I(b)}(L) &= -\frac{eA}{N\hbar} \sum_k \text{Re} \text{Tr} \langle Q_s(L) G_k^R(\mathcal{E}_F) T_\beta G_k^R(\mathcal{E}_F) \rangle, \\ w_{s\beta}^{II}(L) &= \frac{eA}{N\hbar} \sum_k \int_{-\infty}^{\mathcal{E}_F} d\mathcal{E} \text{Re} \text{Tr} \left\langle Q_s(L) G_k^R(\mathcal{E}) T_\beta \frac{dG_k^R(\mathcal{E})}{d\mathcal{E}} \right. \\ &\quad \left. - Q_s(L) \frac{dG_k^R(\mathcal{E})}{d\mathcal{E}} T_\beta G_k^R(\mathcal{E}) \right\rangle, \end{aligned} \quad (108)$$

where we suppressed the  $\hat{M}$  dependence for notational convenience. Comparison of Eqs. (77) and (105) yields the following expression for the spin-mixing conductance:

$$\text{Reg}^{\uparrow\downarrow} = \frac{4\pi}{\hbar A} w_{yy}(L = \text{Co1}), \quad (109)$$

where  $w_{yy}(L = \text{Co1})$  is proportional to spin current flowing between the layers Pt20 and Co1. In Co/Pt bilayers  $t_{yx}^{\text{even}}$  arises almost entirely from the spin flux into the Co layer [31]. The extraction of  $\text{Reg}^{\uparrow\downarrow}$  from  $w_{yy}$  is therefore meaningful in this case despite the presence of SOI in the calculation.

Similarly, as discussed in Sec. III B, SHE provides an important contribution to the even SOT in bilayer systems. The spin currents of the direct SHE are generated by the applied electric field rather than by spin pumping. In order to investigate the layer-resolved spin-current profile of these spin currents in Co(3)/Pt(20), we define the coefficients

$$q_{s\beta}(L, \hat{M}) = A e \lim_{\omega \rightarrow 0} \frac{\text{Im} G_{Q_s(L), v_\beta}^R(\hbar\omega, \hat{M})}{\hbar\omega}. \quad (110)$$

For example,  $q_{yx}(L)$  quantifies the linear response of spin currents flowing in the  $z$  direction with spin pointing in the  $y$  direction to the electric field in the  $x$  direction. Within the independent particle approximation,  $q_{s\beta}(L)$  is expressed similarly to the torkance [Eq. (99)]: only  $T_\alpha$  has to be replaced by  $-A Q_s(L)$  in the expressions.

For a given atomic layer, the difference between spin current flowing in and spin current flowing out is the spin flux into that atomic layer. In Co/Pt bilayer systems, the even SOT arises dominantly from the spin flux into the Co layer [31]. The linear-response coefficient of spin flux into layer  $L$  is given by

$$\Delta q_{yx}(L) = q_{yx}(L) - q_{yx}(L + 1), \quad (111)$$

where according to Eqs. (103) and (110),  $q_{yx}(L)$  describes spin current flowing between layers  $L - 1$  and  $L$  towards layer  $L$  and  $-q_{yx}(L + 1)$  describes spin current flowing between layers  $L$  and  $L + 1$  towards layer  $L$ .

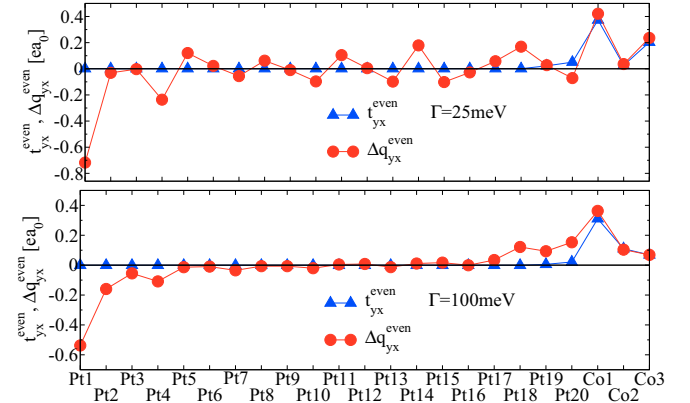


FIG. 1. (Color online) Triangles: layer-resolved even torkance  $t_{yx}^{\text{even}}$  for broadenings of  $\Gamma = 25$  meV (upper graph) and  $\Gamma = 100$  meV (lower graph). Circles: linear-response coefficient of the layer-resolved spin flux  $\Delta q_{yx}^{\text{even}}$  [Eq. (111)]. Solid lines serve as guide to the eye.

## B. Even SOT

We first discuss the even torkance  $t_{yx, 25\text{meV}}^{\text{even}}$  determined from Eq. (99). At  $\Gamma = 25$  meV, we obtain  $t_{yx, 25\text{meV}}^{\text{even}} = 0.68 ea_0$  per unit cell, where  $ea_0$  is the atomic unit of torkance, which amounts to  $ea_0 = 8.478 \times 10^{-30}$  Cm. A slightly smaller value of  $t_{yx, 100\text{meV}}^{\text{even}} = 0.53 ea_0$  is calculated at  $\Gamma = 100$  meV. Dividing these torkances by the magnetic moment per unit cell of  $\mu = 5.78\mu_B$  we compute the effective fields per applied electric field of  $t_{yx, 25\text{meV}}^{\text{even}}/\mu = 0.011$  mT cm/V and  $t_{yx, 100\text{meV}}^{\text{even}}/\mu = 0.0084$  mT cm/V.

In Fig. 1, we show the layer-resolved even torkance, i.e., the linear-response coefficient of the torque acting on the magnetization of a given layer, and the linear-response coefficient of spin flux into layer  $L$  [Eq. (111)]. For the Co layers, layer-resolved torkances and spin fluxes coincide approximately. Thus, the even torkance in Co(3)/Pt(20) arises dominantly from the spin current flowing into the Co layer, consistent with the discussion in Sec. III B and with previous work on Co/Pt bilayer systems [31].

In Fig. 2, we show the linear-response coefficients of the layer-resolved spin current  $q_{yx}^{\text{even}}(L)$  as diamonds for two values of broadening  $\Gamma = 25$  and  $100$  meV [see Eq. (110) for the definition of  $q_{yx}^{\text{even}}(L)$ ]. Evaluating the SHE-to-SOT conversion efficiency defined in Eq. (76) from the ratio of torkance to maximal spin current we obtain  $\xi_{25\text{meV}} = t_{yx}^{\text{even}}/[q_{yx}^{\text{even}}(L = \text{Pt11})] = 0.74$ . At  $\Gamma = 100$  meV, the value is slightly lower:  $\xi_{100\text{meV}} = 0.57$ . These values of  $\xi$  resemble the experimentally determined spin-current transmissivities in Pt-based magnetic bilayer systems [55].

Computing the electric conductivities based on the same formalism as used for SOT and ISOT, we obtain  $\sigma_{xx}^{25\text{meV}} = 1.26 \times 10^7$  S/m and  $\sigma_{xx}^{100\text{meV}} = 0.34 \times 10^7$  S/m. From these conductivities and the spin currents at the center of Pt, which are given by  $q_{yx}^{\text{even}}(L = \text{Pt11})$ , we obtain the following SHE angles:  $\tan \gamma_{\text{SHE}}^{25\text{meV}} = 0.029$  and  $\tan \gamma_{\text{SHE}}^{100\text{meV}} = 0.109$ . The SHE angle increases thus by a factor of 3.8 as  $\Gamma$  is increased from 25 to 100 meV. This increase of the SHE angle with increasing disorder is expected for the intrinsic SHE because the intrinsic



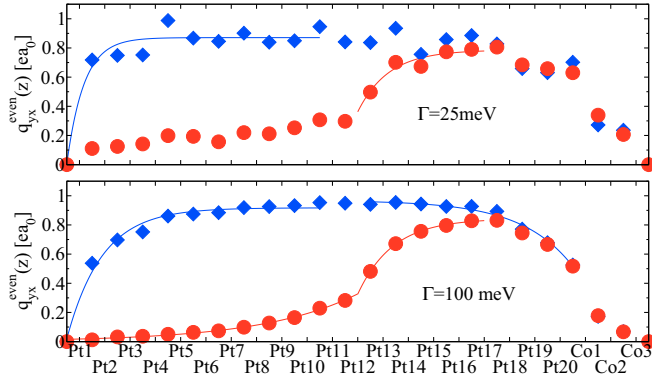


FIG. 2. (Color online) Diamonds: linear-response coefficients  $q_{yx}^{\text{even}}(z)$  of the layer-resolved spin current for  $\Gamma = 25$  meV (upper graph) and  $\Gamma = 100$  meV (lower graph). Circles: linear-response coefficients  $q_{yx}^{\text{even}}(z)$  but with the mechanical force switched off for layers Pt1 through Pt12. Solid lines: exponential fits according to Eqs. (112), (113), (115), and (114).

SHE conductivity  $\sigma_{yx}^y$  [see Eq. (75)] depends only weakly on disorder, while the normal conductivity  $\sigma_{xx}$  decreases with disorder. Indeed, the increase of the SHE angle by the factor of 3.8 is well explained by the ratio  $\sigma_{xx}^{25 \text{ meV}}/\sigma_{xx}^{100 \text{ meV}} = 3.7$ .

At  $\Gamma = 100$  meV, the line of blue diamonds illustrating  $q_{yx}^{\text{even}}(z)$  in Fig. 2 is constant in the central region between Pt5 and Pt15 because the primary spin current generated by SHE is constant in this region and because secondary spin currents arising from the reflections of spin current at the surfaces and interfaces decay strongly spatially and therefore do not reach the central region between Pt5 and Pt15. One reason for the suppression of the spin-current profile in the region between Pt1 and Pt5 and in the region between Pt15 and Pt20 is the interference of the primary spin current from the SHE with secondary spin current reflected, respectively, from the surface and the interface. Additionally, as discussed in Sec. III B, we expect that the primary spin current generated by the SHE is itself dependent on position in these two regions and not constant as in the central region. In particular, for the higher broadening of  $\Gamma = 100$  meV the spin-current profiles from our *ab initio* calculations shown in Fig. 2 exhibit exponential behavior in the regions Pt1 through Pt5 and in the regions Pt15 through Pt20. At  $\Gamma = 100$  meV, the spin current in the region between Pt12 and Co1 is well described by the exponential fit

$$q_{yx}^{\text{even}}(z) = [0.97 - 0.35e^{(z-z_{\text{Pt20}})/\lambda_{\text{SOT},3}^{100 \text{ meV}}}]ea_0, \quad (112)$$

where  $z_{\text{Pt20}}$  is the  $z$  coordinate of layer Pt20 and  $\lambda_{\text{SOT},3}^{100 \text{ meV}} = 0.46$  nm. In the region from Pt1 to Pt10, the spin current is approximately given by

$$q_{yx}^{\text{even}}(z) = [0.92 - 0.63e^{-(z-z_{\text{Pt1}})/\lambda_{\text{SOT},4}^{100 \text{ meV}}}]ea_0 \quad (113)$$

with  $\lambda_{\text{SOT},4}^{100 \text{ meV}} = 0.32$  nm. At the smaller broadening of  $\Gamma = 25$  meV, we find  $\lambda_{\text{SOT},4}^{25 \text{ meV}} = 0.15$  nm, but due to oscillations the first-principles data are less well described by the exponential fit.

The length  $\lambda_{\text{SOT},4}^{100 \text{ meV}}$  describes the decay of spin current close to the vacuum boundary at Pt1, while the length  $\lambda_{\text{SOT},3}^{100 \text{ meV}}$  describes the decay of spin current close to the Co layer.

In order to investigate whether  $\lambda_{\text{SOT},4}^{100 \text{ meV}}$  and  $\lambda_{\text{SOT},3}^{100 \text{ meV}}$  simply describe the decay of secondary reflected spin current or whether they additionally exhibit a modification due to a potential position dependence of the primary spin current, we divide the Pt layer into two regions: In the atomic layers Pt1 through Pt12 we switch off the mechanical force  $-e\mathbf{E}$  that the electrons would otherwise experience due to the applied electric field  $\mathbf{E}$ . Only the atomic layers Pt13 through Co3 are subject to the mechanical force  $-e\mathbf{E}$  in this modified calculation, which is based on Eq. (102). Thus, only Pt13 through Pt20 generate sizable SHE spin current (SHE in Co is small). The corresponding linear-response coefficients are shown in Fig. 2 as circles for two values of broadening,  $\Gamma = 25$  and 100 meV. Switching off the mechanical force significantly perturbs the spin-current profile in the region Pt1 through Pt14 while from Pt15 onwards, the two spin-current profiles merge. Approaching the region with mechanical force switched off, i.e., approaching Pt12, the spin current (red circles in Fig. 2) in region Pt13 to Pt17 is suppressed according to

$$q_{yx}^{\text{even}}(z) = [0.84 - 0.52e^{-(z-z_{\text{Pt12}})/\lambda_{\text{SOT},5}^{100 \text{ meV}}}]ea_0, \quad (114)$$

where  $\lambda_{\text{SOT},5}^{100 \text{ meV}} = 0.31$  nm. We find a slight  $\Gamma$  dependence:  $\lambda_{\text{SOT},5}^{25 \text{ meV}} = 0.28$  nm. In the region from Pt1 through Pt12, the spin current is well described by

$$q_{yx}^{\text{even}}(z) = 0.33e^{(z-z_{\text{Pt12}})/\lambda_{\text{SOT},2}^{100 \text{ meV}}}ea_0, \quad (115)$$

with  $\lambda_{\text{SOT},2}^{100 \text{ meV}} = 0.85$  nm. At  $\Gamma = 25$  meV, the spin-current profile in the region Pt1 through Pt14 cannot be described well by an exponential fit.

Comparing the lengths obtained from the exponential fits in Eqs. (112), (113), (115), and (114), we find that  $\lambda_{\text{SOT},2}^{100 \text{ meV}}$  is substantially larger than the other three lengths:  $\lambda_{\text{SOT},2}^{100 \text{ meV}} > \lambda_{\text{SOT},3}^{100 \text{ meV}} \approx \lambda_{\text{SOT},4}^{100 \text{ meV}} \approx \lambda_{\text{SOT},5}^{100 \text{ meV}}$ . The length  $\lambda_{\text{SOT},2}^{100 \text{ meV}}$  describes the decay of spin current in Pt in a region of space where no spin current is generated (because the mechanical force is switched off in the regions Pt1 through Pt12). This spin current, which is injected into the regions Pt1–Pt12, originates only from the SHE in the regions Pt13–Pt20. In contrast, the lengths  $\lambda_{\text{SOT},3}^{100 \text{ meV}}$ ,  $\lambda_{\text{SOT},4}^{100 \text{ meV}}$ , and  $\lambda_{\text{SOT},5}^{100 \text{ meV}}$  describe the suppression of the total spin current close to interfaces and surfaces. The total spin current is the sum of spin current generated by SHE and spin current from the reflection at interfaces and surfaces. This reflected spin current is expected to be described by  $\lambda_{\text{SOT},2}^{100 \text{ meV}}$ . Our finding that  $\lambda_{\text{SOT},3}^{100 \text{ meV}}$ ,  $\lambda_{\text{SOT},4}^{100 \text{ meV}}$ , and  $\lambda_{\text{SOT},5}^{100 \text{ meV}}$  are all much smaller than  $\lambda_{\text{SOT},2}^{100 \text{ meV}}$  can only be explained if we assume that the primary spin current generated by SHE is itself modified close to surfaces and interfaces.

In Fig. 3, we show the torkance as a function of the region where the mechanical force is set to zero. If the mechanical force is switched off in all Pt layers and only active in the Co layers (data points at  $L = \text{Co1}$ ),  $t_{yx}^{\text{even}}$  is very small because the even torque arises dominantly from the SHE in Pt which is switched off when the mechanical force is set to zero. When the mechanical force is set to zero in the region from Pt1 through layer  $L - 1$ , the torkance is well described by the fit

$$t_{yx}^{\text{even}}(z) = [0.65 - 0.68e^{-(z_{\text{Co1}}-z)/\lambda_{\text{SOT},1}^{25 \text{ meV}}}]ea_0, \quad (116)$$

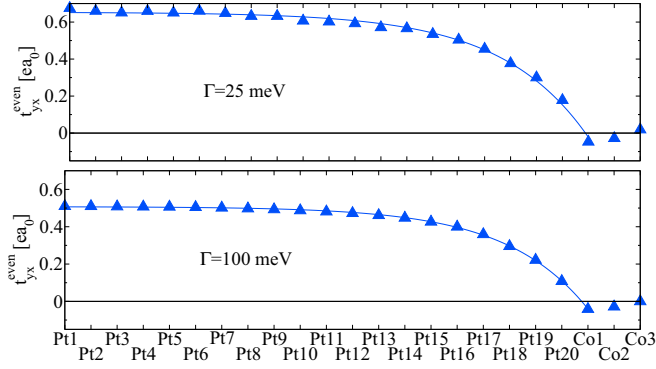


FIG. 3. (Color online) Triangles: torkances for broadenings of  $\Gamma = 25$  meV (upper graph) and  $\Gamma = 100$  meV (lower graph). For a given layer  $L$  ( $L$  is specified on the horizontal axis), the mechanical force is switched off in the region from Pt1 through  $L - 1$  according to Eq. (102) and the resulting total torkance is shown by a blue triangle. Solid lines: exponential fits according to Eq. (116).

where  $\lambda_{\text{SOT},1}^{25 \text{ meV}} = 0.76$  nm. We find a weak  $\Gamma$  dependence:  $\lambda_{\text{SOT},1}^{100 \text{ meV}} = 0.71$  nm. At  $\Gamma = 100$  meV, the spin current generated in a given atomic layer of Pt decays on the length scale of  $\lambda_{\text{SOT},2}^{100 \text{ meV}}$ . Therefore, the SHE from layers  $L$  that are further away from the Co layer than  $\lambda_{\text{SOT},2}^{100 \text{ meV}}$  cannot contribute to  $t_{yx}^{\text{even}}$ . Thus, we expect  $\lambda_{\text{SOT},1}^{100 \text{ meV}} \approx \lambda_{\text{SOT},2}^{100 \text{ meV}}$ , which is indeed the case.

One main conclusion of this section is that for a sufficiently large broadening  $\Gamma = 100$  meV, the *ab initio* spin-current profiles behave as expected from diffusive spin-transport models. In particular, at  $\Gamma = 100$  meV, the decay lengths of spin current extracted in various ways are found to be similar, namely,  $\lambda_{\text{SOT},1}^{100 \text{ meV}} = 0.71$  nm and  $\lambda_{\text{SOT},2}^{100 \text{ meV}} = 0.85$  nm. Similarly short but slightly longer length scales of roughly 1.5 nm have been observed in Pt in recent experiments [22,38,63,64]. A second conclusion from this section is that close to interfaces and surfaces, the SHE conductivity is position dependent. Therefore, close to interfaces and surfaces, the spin-current profiles do not decay on the scale of  $\lambda_{\text{SOT},1}^{100 \text{ meV}} \approx \lambda_{\text{SOT},2}^{100 \text{ meV}}$  but instead significantly faster, namely, according to  $\lambda_{\text{SOT},3}^{100 \text{ meV}} \approx \lambda_{\text{SOT},4}^{100 \text{ meV}} \approx \lambda_{\text{SOT},5}^{100 \text{ meV}} \approx 0.3$  nm.

### C. Even ISOT

When the magnetization precesses in a circular orbit around the  $z$  axis in the small-cone limit, the current density

$$\begin{aligned} \frac{J_{x,25 \text{ meV}}^{\text{even}}(t)}{\omega} &= -87 \frac{\text{pAs}}{\text{m}} \sin(\theta) \sin(\omega t), \\ \frac{J_{x,100 \text{ meV}}^{\text{even}}(t)}{\omega} &= -68 \frac{\text{pAs}}{\text{m}} \sin(\theta) \sin(\omega t) \end{aligned} \quad (117)$$

is induced due to the even torkance  $t_{yx}^{\text{even}}$  according to Eq. (68), where we used  $A_0 = t_{yx}^{\text{even}}$  and  $A = 23.8 a_0^2$ .

As discussed in Sec. III B, the ISOT current  $I_x^{\text{even}} = J_x^{\text{even}} L_y$  arises dominantly from the combination of spin pumping and ISHE. Since the spin current pumped into Pt decays, the layer-resolved ISOT current  $I_x^{\text{even}}(L)$  is expected to reflect this spatial decay. Replacing  $v_\alpha$  in Eq. (99) by  $v_\alpha(L)$

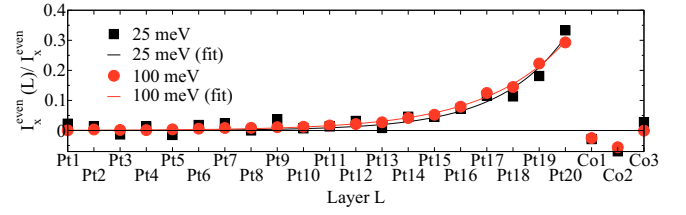


FIG. 4. (Color online) Layer-resolved ISOT current  $I_x^{\text{even}}(L)$  induced in Co(3)/Pt(20) by magnetization dynamics. The total ISOT current is  $I_x^{\text{even}} = \sum_L I_x^{\text{even}}(L)$ . The relative contributions of the layers, i.e.,  $I_x^{\text{even}}(L)/I_x^{\text{even}}$ , is shown for two values of broadening,  $\Gamma = 25$  and 100 meV. Solid lines: exponential fit according to Eq. (118).

[Eq. (100)] yields the layer-resolved ISOT current  $I_x^{\text{even}}(L)$  shown in Fig. 4. Inside the Pt layer,  $I_x^{\text{even}}(L)$  is well described by an exponential function

$$I_x^{\text{even}}(z) = I_x^{\text{even}}(z_{\text{Pt20}}) e^{(z - z_{\text{Pt20}})/\lambda_{\text{ISOT},1}}, \quad (118)$$

where  $z_{\text{Pt20}}$  is the  $z$  coordinate of layer Pt20. Fitting Eq. (118) to the  $I_x^{\text{even}}(L)$  profile obtained from first principles yields  $\lambda_{\text{ISOT},1}^{25 \text{ meV}} = 0.58$  nm and  $\lambda_{\text{ISOT},1}^{100 \text{ meV}} = 0.70$  nm.

In order to compare the spatial profile of the layer-resolved ISOT current  $I_x^{\text{even}}(L)$  with the spatial profile of the pumped spin current  $Q_y(L, t)$  given by Eq. (105), we calculate the coefficients  $w_{yy}(L)$ , which are defined in Eq. (108).  $w_{yy}(L)$  describes spin current in phase with  $I_x^{\text{even}}$  and with spin pointing in the  $y$  direction. Within Pt, the  $L$  dependence of  $w_{yy}(L)$ , shown in Fig. 5, is approximately given by

$$w_{yy}(z) = 0.087 h e^{(z - z_{\text{Pt20}})/\lambda_{\text{ISOT},2}^{100 \text{ meV}}}, \quad (119)$$

where  $\lambda_{\text{ISOT},2}^{100 \text{ meV}} = 0.89$  nm. At smaller broadening  $\Gamma = 25$  meV, the pumped spin current reaches the vacuum boundary at Pt1 and the resulting reflection of spin current needs to be considered according to Eq. (86). When  $\lambda_{\text{ISOT},2}^{25 \text{ meV}}$  is much larger than the thickness of Pt, the sinh function can be approximated:

$$w_{yy}(z) \propto \frac{\sinh \frac{z - z_{\text{Pt1}}}{\lambda_{\text{ISOT},2}^{25 \text{ meV}}}}{\sinh \frac{z_{\text{Pt20}} - z_{\text{Pt1}}}{\lambda_{\text{ISOT},2}^{25 \text{ meV}}}} \approx \frac{z - z_{\text{Pt1}}}{z_{\text{Pt20}} - z_{\text{Pt1}}}, \quad (120)$$

which explains the roughly linear profile of  $w_{yy}(L)$  at  $\Gamma = 25$  meV.

The ISOT currents shown in Fig. 4 decay faster in Pt than the spin currents in Fig. 5. Thus, Eq. (80), which predicts spin

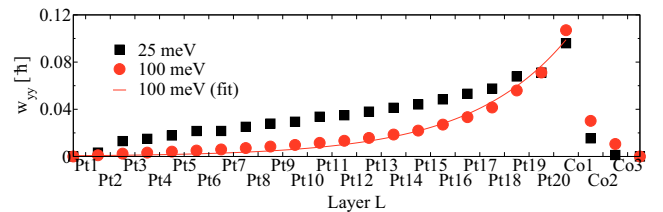


FIG. 5. (Color online) Layer-resolved spin current induced by magnetization dynamics for two values of broadening,  $\Gamma = 25$  and 100 meV. The coefficient  $w_{yy}$  describes spin current flowing in  $z$  direction with spin pointing in  $y$  direction and in phase with  $I_x^{\text{even}}(t)$ . Solid line: fit according to Eq. (119).

current and ISHE current to be proportional, is violated, in particular at  $\Gamma = 25$  meV. However, Eq. (80) is approximately satisfied at  $\Gamma = 100$  meV, where both the ISOT current and the pumped spin current decay exponentially with  $\lambda_{\text{ISOT},1}^{100 \text{ meV}} \approx \lambda_{\text{ISOT},2}^{100 \text{ meV}}$ . The small difference  $\lambda_{\text{ISOT},2}^{100 \text{ meV}} - \lambda_{\text{ISOT},1}^{100 \text{ meV}} = 0.19$  nm amounts to less than one Pt interlayer distance. Additionally, this spin-current decay length  $\lambda_{\text{ISOT},1}^{100 \text{ meV}} \approx \lambda_{\text{ISOT},2}^{100 \text{ meV}}$  is very similar to the one extracted in the previous subsection, i.e.,  $\lambda_{\text{ISOT},1}^{100 \text{ meV}} \approx \lambda_{\text{ISOT},2}^{100 \text{ meV}} \approx \lambda_{\text{SOT},1}^{100 \text{ meV}} \approx \lambda_{\text{SOT},2}^{100 \text{ meV}}$ . This consistency between the various methods used to extract the spin-current decay length implies that the model of Sec. III B provides a satisfactory description at sufficiently high broadening  $\Gamma$ .

In Eq. (79), the ISHE angle  $\tan \gamma_{\text{ISHE}}$  is proportional to the quotient of ISOT current density and pumped spin-current density. The different decay of ISOT current and pumped spin current described by  $\lambda_{\text{ISOT},1}^{100 \text{ meV}}$  and  $\lambda_{\text{ISOT},2}^{100 \text{ meV}}$ , respectively, therefore implies that  $\tan \gamma_{\text{ISHE}}$  is not constant but dependent on position. For large broadening, we obtain  $\tan \gamma_{\text{ISHE}}^{100 \text{ meV}}(L = \text{Pt20}) = 0.16$  and  $\tan \gamma_{\text{ISHE}}^{100 \text{ meV}}(L = \text{Pt11}) = 0.077$ , while for small broadening we obtain  $\tan \gamma_{\text{ISHE}}^{25 \text{ meV}}(L = \text{Pt20}) = 0.27$  and  $\tan \gamma_{\text{ISHE}}^{25 \text{ meV}}(L = \text{Pt11}) = 0.031$ . Even for large broadening, the ISHE angle is significantly enhanced at the interface. The ISHE angles at the center of Pt, i.e.,  $\tan \gamma_{\text{ISHE}}^{100 \text{ meV}}(L = \text{Pt11})$  and  $\tan \gamma_{\text{ISHE}}^{25 \text{ meV}}(L = \text{Pt11})$ , are similar to the SHE angles determined in the previous section from the spin current in the center of Pt:  $\tan \gamma_{\text{SHE}}^{100 \text{ meV}}(L = \text{Pt11}) = 0.109$  and  $\tan \gamma_{\text{SHE}}^{25 \text{ meV}}(L = \text{Pt11}) = 0.029$ .

From Eq. (109), we obtain the spin-mixing conductance  $\text{Reg}_{25 \text{ meV}}^{\uparrow\downarrow} = 1.8 \times 10^{19} \text{ m}^{-2}$  and for  $\Gamma = 100$  meV a slightly larger value of  $\text{Reg}_{100 \text{ meV}}^{\uparrow\downarrow} = 2.0 \times 10^{19} \text{ m}^{-2}$ . Equation (84) provides an alternative way to extract the ISHE angle:

$$\tan \tilde{\gamma}_{\text{ISHE}}^{100 \text{ meV}} = \frac{2\pi t_{yx}^{\text{even}}}{eA \text{Reg}_{100 \text{ meV}}^{\uparrow\downarrow} \lambda_{\text{ISOT},2}^{100 \text{ meV}}} = 0.15, \quad (121)$$

where the in-plane area of the unit cell is  $A = 23.8 a_0^2$  and the parameters  $\lambda_{\text{ISOT},2}^{100 \text{ meV}} = 0.89$  nm and  $t_{yx}^{\text{even}} = 0.53 e a_0$  have been discussed above. In contrast to the layer-resolved ISHE angles, Eq. (121) describes an average over all those Pt layers that lie within the distance of  $\lambda_{\text{ISOT},2}^{100 \text{ meV}}$  from the Co layer. The result of  $\tan \tilde{\gamma}_{\text{ISHE}}^{100 \text{ meV}} = 0.15$  is very similar to the layer-resolved ISHE angle close to the interface of  $\tan \gamma_{\text{ISHE}}^{100 \text{ meV}}(L = \text{Pt20}) = 0.16$ .

Finally, we can also put Eq. (85) to a test using the parameters determined above:

$$\lambda_{\text{sd}}^{100 \text{ meV}} = \frac{\xi_{100 \text{ meV}} \hbar \pi \sigma_{xx}^{100 \text{ meV}}}{e^2 \text{Reg}_{100 \text{ meV}}^{\uparrow\downarrow}} = 1.25 \text{ nm}. \quad (122)$$

While  $\lambda_{\text{sd}}^{100 \text{ meV}}$  is larger than  $\lambda_{\text{ISOT},2}^{100 \text{ meV}}$ , the agreement between these two values is still satisfactory, corroborating the conclusion that the model of Sec. III B provides a satisfactory description for sufficiently large broadening. For small broadening, Eq. (85) yields  $\lambda_{\text{sd}}^{25 \text{ meV}} = 6.7$  nm, which is thicker than the Pt layer in our calculation and therefore justifies the linear approximation in Eq. (120).

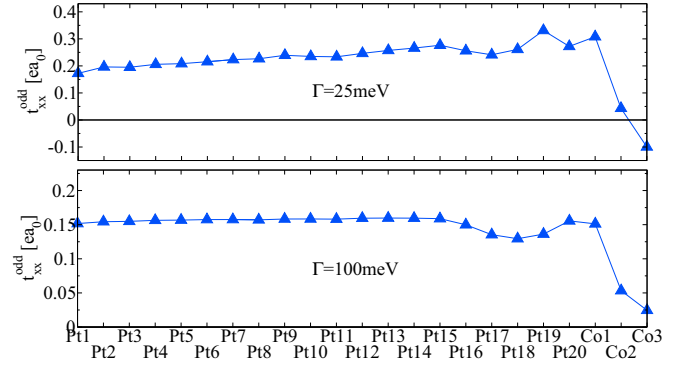


FIG. 6. (Color online) Triangles: torkances for broadenings of  $\Gamma = 25$  meV (upper graph) and  $\Gamma = 100$  meV (lower graph). For a given layer  $L$  ( $L$  is specified on the horizontal axis), the mechanical force is switched off in the region from Pt1 through  $L - 1$  according to Eq. (102) and the resulting total torkance is shown by a blue triangle. Solid lines serve as guide to the eye.

#### D. Odd SOT

We obtain torkances per unit cell of  $t_{xx,25 \text{ meV}}^{\text{odd}} = 0.17 e a_0$  and  $t_{xx,100 \text{ meV}}^{\text{odd}} = 0.15 e a_0$  at broadenings of  $\Gamma = 25$  and  $100$  meV, respectively. Dividing these torkances by the magnetic moment per unit cell of  $\mu = 5.78 \mu_B$  we calculate the effective fields per applied electric field of  $t_{xx,25 \text{ meV}}^{\text{odd}}/\mu = 0.0027 \text{ mT cm/V}$  and  $t_{xx,100 \text{ meV}}^{\text{odd}}/\mu = 0.0024 \text{ mT cm/V}$ .

In Fig. 6, we show the odd torkance as a function of the region with mechanical force switched off. If the mechanical force is switched off for Pt1 through Pt20 such that only the layers Co1, Co2, and Co3 are subject to it (see the data points at  $L = \text{Co1}$  in the figure), the corresponding odd torque is not very different from the one with the mechanical force switched on everywhere (see the data points at  $L = \text{Pt1}$  in the figure). If the mechanical force is applied only to layers Co2 and Co3 (see data points at  $L = \text{Co2}$  in the figure), the resulting torkance is much smaller compared to the situation where all three Co layers are subject to it. Thus, the perturbation of the Co1 layer by the mechanical force is essential for the odd SOT in this system.

To produce a sizable odd torque in Co(3)/Pt(20), it is therefore not crucial to switch on the mechanical force in the Pt layers but it suffices to apply this perturbation to the Co states. As a combined effect of broken inversion symmetry and SOI, the spin of a given wave function  $|\Psi_{kn}\rangle$  is correlated with the velocity  $v_{kn}$  [65]. As a result, the nonequilibrium spin density induced by an applied electric field combined with the exchange interaction gives rise to the odd component of the torkance [9,10,66]. Application of the mechanical force to Co, i.e., perturbation of the system via the velocity operator within the Co layer, produces therefore the dominant part of nonequilibrium spin density from which the odd torque arises in Co(3)/Pt(20). This stands in marked contrast to the even torque in this system, which is mainly driven by SHE from Pt and thus very small if the mechanical force is turned off in all Pt layers, as shown in Fig. 3.

In Fig. 7, the layer-resolved odd torkance and the linear-response coefficient of spin flux into layer  $L$ , i.e.,

$$\Delta q_{xx}^{\text{odd}}(L) = q_{xx}^{\text{odd}}(L) - q_{xx}^{\text{odd}}(L + 1), \quad (123)$$

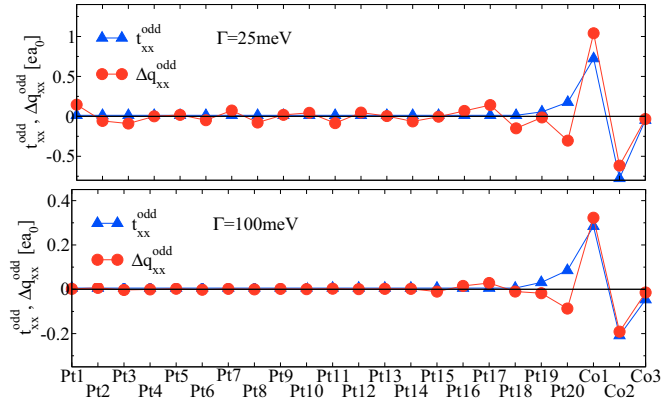


FIG. 7. (Color online) Triangles: layer-resolved odd torque  $t_{xx}^{\text{odd}}$  for broadenings of  $\Gamma = 25$  meV (upper graph) and  $\Gamma = 100$  meV (lower graph). Circles: linear-response coefficient of the layer-resolved spin flux  $\Delta q_{xx}^{\text{odd}}$  [Eq. (123)]. Solid lines serve as guide to the eye.

are shown for two values of broadening,  $\Gamma = 25$  and  $100$  meV. For the layers Co1 through Co3, the layer-resolved torques coincide approximately with the spin fluxes as in the case of the even torque. This approximate agreement between odd spin fluxes and odd torques is not generally found in bilayer systems, for example, they differ considerably in O/Co/Pt and Al/Co/Pt [31]. For  $\Gamma = 100$  meV, the magnetization of layer Pt20 experiences a torque of  $0.085ea_0$ . At the same time, there is a spin flux out of layer Pt20 characterized by the coefficient  $-\Delta q_{xx}^{\text{odd}}(L = \text{Pt20}) = 0.087ea_0$ . This spin flux is transferred to the Co layer where it exerts a torque on the Co magnetization. The sum of torque and spin-flux coefficient of Pt20 amounts to  $0.172ea_0$  and approximately accounts for the total odd torque of  $0.15ea_0$  at  $\Gamma = 100$  meV. The angular momentum that gives rise to the odd torque on the magnetization is thus picked up from the lattice at Pt20 and roughly 50% of it is directly transferred to the magnetization of the Pt20 layer while the rest is transported to the Co layer via spin current. Above, we have shown that the mechanical force on the Co1 layer is crucial to produce a sizable odd torque. Since the pickup of angular momentum from the lattice by the spin system happens in Pt20, the hybridization of the Co1 states with the Pt20 states is thus essential.

### E. Odd ISOT

According to Eq. (68), the current density

$$\begin{aligned} \frac{J_{x,25\text{ meV}}^{\text{odd}}(t)}{\omega} &= 22 \frac{\text{pAs}}{\text{m}} \sin(\theta) \cos(\omega t), \\ \frac{J_{x,100\text{ meV}}^{\text{odd}}(t)}{\omega} &= 19 \frac{\text{pAs}}{\text{m}} \sin(\theta) \cos(\omega t) \end{aligned} \quad (124)$$

is induced due to  $t_{xx}^{\text{odd}}$  when the magnetization precesses around the  $z$  axis in the small-cone limit. Here, we used  $C_0 = t_{xx}^{\text{odd}}$  and  $A = 23.8a_0^2$ . This contribution from  $t_{xx}^{\text{odd}}$  is thus  $-90^\circ$  phase shifted with respect to the contribution from  $t_{yx}^{\text{even}}$  given in Eq. (117), i.e., it lags behind by a quarter period.

Since the mechanical force on the Co1 layer is crucial for the odd SOT according to Fig. 6, we expect that the odd ISOT

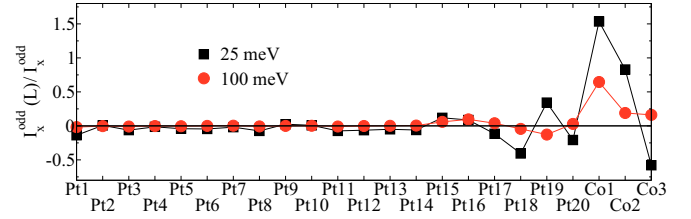


FIG. 8. (Color online) Layer-resolved ISOT current  $I_x^{\text{odd}}(L)$  induced in Co(3)/Pt(20) by magnetization dynamics. The total ISOT current is  $I_x^{\text{odd}} = \sum_L I_x^{\text{odd}}(L)$ . The relative contributions of the layers, i.e.,  $I_x^{\text{odd}}(L)/I_x^{\text{odd}}$ , is shown for two values of broadening,  $\Gamma = 25$  meV (squares) and  $\Gamma = 100$  meV (circles). Solid lines serve as guide to the eye.

current induced by magnetization dynamics flows mainly in the Co1 layer because of the reciprocity between ISOT and SOT. This is indeed the case, as Fig. 8 shows. In particular, at  $\Gamma = 100$  meV, the currents flowing in Co2, Co3, and the Pt layer are almost negligible. At the smaller broadening  $\Gamma = 25$  meV, the induced ISOT currents in Co2, Co3, and Pt are larger, especially in the Co2 and Co3 layers, but the Co1 contribution to the ISOT current still strongly dominates.

## V. SUMMARY

SOT and ISOT are reciprocal effects. Both of them can be expressed conveniently in terms of the torque tensor  $\mathbf{t}(\hat{\mathbf{M}})$ , which depends on the magnetization direction  $\hat{\mathbf{M}}$ . In the case of the SOT phenomenon, the torque  $\mathbf{T}(\hat{\mathbf{M}})$  on the magnetization due to the application of an electric field  $\mathbf{E}$  is given by  $\mathbf{T}(\hat{\mathbf{M}}) = \mathbf{t}(\hat{\mathbf{M}})\mathbf{E}$ . If  $\hat{\mathbf{M}}$  changes as a function of time, the reciprocal effect, the ISOT, can be observed. It consists in the generation of a current density  $\mathbf{j}(t) = \{\mathbf{t}(-\hat{\mathbf{M}}(t))\}^T [\hat{\mathbf{M}}(t) \times \frac{d\hat{\mathbf{M}}(t)}{dt}] / V$ , where  $V$  is the unit-cell volume. Magnetization-dynamics-driven effects, such as ISOT and Gilbert damping, can be consistently derived in time-dependent perturbation theory using a time-dependent exchange field. The same expressions are obtained by rewriting general many-body susceptibilities in terms of the Kohn-Sham susceptibilities. On the basis of the SOT-ISOT reciprocity relations and recent experimental results for the SOT in bilayer systems, we predict the angular dependence of the FMR-driven ISOT in bilayers. We find that measurements of the dc voltage associated with the FMR-driven ISOT are insufficient to determine  $\mathbf{t}(\hat{\mathbf{M}})$  in general and that additionally the ac voltage needs to be measured phase sensitively to determine  $\mathbf{t}(\hat{\mathbf{M}})$  completely. Within the Kubo linear-response formalism, we investigate SOTs and ISOTs in Co/Pt(111) magnetic bilayers using the electronic structure provided from first-principles density-functional theory. Magnetization-dynamics-induced charge currents and spin currents are resolved on the atomic scale to extract model parameters and to expose the mechanisms underlying the ISOT. Likewise, the spin currents accompanying the SOT are resolved on the atomic scale for the same purposes. It is found that SHE and ISHE are modified close to interfaces and surfaces. Comparison of the various currents accompanying SOT on the one hand and ISOT on the other hand highlights the reciprocity of the two phenomena on the microscopic scale.



## ACKNOWLEDGMENTS

We gratefully acknowledge computing time on the supercomputers JUQUEEN and JUROPA at Jülich Supercomputing Center and funding under the Helmholtz-Gemeinschaft Deutscher Forschungszentren (HGF)-Young Investigator Group (YIG) programme VH-NG-513.

## APPENDIX: MAGNETOCRYSTALLINE ANISOTROPY AND THE STATIC TORQUE-TORQUE CORRELATION FUNCTION

The torque due to the field  $\mathbf{H}^{\text{MAE}}$  [Eq. (30)] is given by

$$\begin{aligned}\delta\mathbf{T}^{\text{MAE}} &= \mu_0 M V \hat{\mathbf{M}} \times \mathbf{H}^{\text{MAE}} \\ &= -M V \left[ \bar{\Omega}^{\text{xc}} + \frac{G_{\mathcal{T}\mathcal{T}}^{\text{R}}(\hbar\omega = 0, \hat{\mathbf{M}})}{M V \hbar} \right] \hat{\mathbf{M}} \times \delta\hat{\mathbf{M}},\end{aligned}\quad (\text{A1})$$

where we used Eq. (48) to express  $\chi$  in terms of the torque-torque correlation function  $G_{\mathcal{T}\mathcal{T}}^{\text{R}}$ . Equation (A1) can be related easily to anisotropy constants. For example, in the case of uniaxial anisotropy, i.e.,  $E(\theta) = V K_1 \sin^2 \theta$ , one obtains

$$K_1 = \frac{M}{2} \left[ \bar{\Omega}^{\text{xc}} + \frac{G_{\mathcal{T}_y\mathcal{T}_y}^{\text{R}}(\hbar\omega = 0, \hat{\mathbf{M}} = \hat{\mathbf{e}}_z)}{M V \hbar} \right]. \quad (\text{A2})$$

In the following, we show that Eq. (A1), which was obtained within the many-electron response formalism of Sec. II C, can also be obtained directly from the torque exerted on the magnetization by the Kohn-Sham electrons. Denoting the Kohn-Sham wave functions by  $|\psi_{kn}\rangle$  and the occupancies by  $f_{kn}$  we can write

$$\begin{aligned}\delta\mathbf{T}^{\text{MAE}} &= -\delta \left\{ \frac{1}{\mathcal{N}} \sum_{kn} f_{kn} \langle \psi_{kn} | \mathcal{T} | \psi_{kn} \rangle \right\} \\ &= -\frac{1}{\mathcal{N}} \sum_{kn} f_{kn} \langle \psi_{kn} | \delta\mathcal{T} | \psi_{kn} \rangle \\ &\quad - \frac{1}{\mathcal{N}} \sum_{kn} \delta f_{kn} \langle \psi_{kn} | \mathcal{T} | \psi_{kn} \rangle \\ &\quad - 2 \text{Re} \frac{1}{\mathcal{N}} \sum_{kn} f_{kn} \langle \psi_{kn} | \mathcal{T} \delta | \psi_{kn} \rangle.\end{aligned}\quad (\text{A3})$$

From  $\delta\mathcal{T} = \mathbf{m} \times \delta\hat{\mathbf{M}}\Omega^{\text{xc}}$  we obtain for the first term

$$-\frac{1}{\mathcal{N}} \sum_{kn} f_{kn} \langle \psi_{kn} | \delta\mathcal{T} | \psi_{kn} \rangle = -M V \bar{\Omega}^{\text{xc}} \hat{\mathbf{M}} \times \delta\hat{\mathbf{M}}. \quad (\text{A4})$$

Using for the remaining terms

$$\delta|\psi_{kn}\rangle = \sum_{m \neq n} \frac{|\psi_{km}\rangle \langle \psi_{km} | \mathcal{T} | \psi_{kn} \rangle}{\mathcal{E}_{kn} - \mathcal{E}_{km}} \cdot (\hat{\mathbf{M}} \times \delta\hat{\mathbf{M}}) \quad (\text{A5})$$

and

$$\delta f_{kn} = -\delta(\mathcal{E}_{\text{F}} - \mathcal{E}_{kn}) \langle \psi_{kn} | \mathcal{T} | \psi_{kn} \rangle \cdot (\hat{\mathbf{M}} \times \delta\hat{\mathbf{M}}) \quad (\text{A6})$$

and

$$\begin{aligned}G_{\mathcal{T}_\alpha\mathcal{T}_\beta}^{\text{R}} &= \frac{2\hbar}{\mathcal{N}} \sum_{kn} \sum_{m \neq n} f_{kn} \text{Re} \frac{\langle \psi_{kn} | \mathcal{T}_\alpha | \psi_{km} \rangle \langle \psi_{km} | \mathcal{T}_\beta | \psi_{kn} \rangle}{\mathcal{E}_{kn} - \mathcal{E}_{km}} \\ &\quad - \frac{\hbar}{\mathcal{N}} \sum_{kn} \delta(\mathcal{E}_{\text{F}} - \mathcal{E}_{kn}) \langle \psi_{kn} | \mathcal{T}_\alpha | \psi_{kn} \rangle \langle \psi_{kn} | \mathcal{T}_\beta | \psi_{kn} \rangle,\end{aligned}\quad (\text{A7})$$

one can easily show that Eqs. (A1) and (A3) agree.

The Kohn-Sham Hamiltonian can be decomposed as

$$H(\mathbf{r}) = H_{\text{KIN}} + V(\mathbf{r}) - \mathbf{m} \cdot \hat{\mathbf{M}}\Omega^{\text{xc}}(\mathbf{r}) + H_{\text{SOI}}, \quad (\text{A8})$$

where  $H_{\text{KIN}}$  describes the kinetic energy,  $V(\mathbf{r})$  is the spin-independent part of the effective potential, and  $H_{\text{SOI}}$  describes the spin-orbit interaction. Using  $[H_{\text{KIN}}, \sigma_\beta] = 0$ ,  $[V(\mathbf{r}), \sigma_\beta] = 0$ , and  $[\sigma_\alpha, \sigma_\beta] = 2i\epsilon_{\alpha\beta\gamma}\sigma_\gamma$ , one can show the following identity for the torque operator:

$$\mathcal{T}_\beta = \frac{i}{2} [H - H_{\text{SOI}}, \sigma_\beta]. \quad (\text{A9})$$

Substituting  $\mathcal{T}_\beta$  in Eq. (A7) by Eq. (A9) and inserting the resulting expression for  $G_{\mathcal{T}_\alpha\mathcal{T}_\beta}^{\text{R}}$  into Eq. (A1) we obtain

$$\begin{aligned}\delta\mathbf{T}^{\text{MAE}} &= -\frac{1}{\mathcal{N}} \sum_{kn\beta} (\hat{\mathbf{M}} \times \delta\hat{\mathbf{M}})_\beta \\ &\quad \times \left\{ f_{kn} \text{Im} \sum_{m \neq n} \frac{\langle \psi_{kn} | \mathcal{T} | \psi_{km} \rangle \langle \psi_{km} | [H_{\text{SOI}}, \sigma_\beta] | \psi_{kn} \rangle}{\mathcal{E}_{kn} - \mathcal{E}_{km}} \right. \\ &\quad \left. + \frac{i}{2} \delta(\mathcal{E}_{\text{F}} - \mathcal{E}_{kn}) \langle \psi_{kn} | \mathcal{T} | \psi_{kn} \rangle \langle \psi_{kn} | [H_{\text{SOI}}, \sigma_\beta] | \psi_{kn} \rangle \right\}.\end{aligned}\quad (\text{A10})$$

Equation (A10) is well suited for the calculation of the magnetocrystalline anisotropy within Kohn-Sham density-functional-theory codes. In contrast, the direct application of Eq. (A1) in practice would suffer from the following disadvantage: Since the magnetocrystalline anisotropy energy is usually much smaller than the average exchange field  $\bar{\Omega}^{\text{xc}}$ , one would need to calculate both  $\bar{\Omega}^{\text{xc}}$  as well as the torque-torque correlation function  $G_{\mathcal{T}_\alpha\mathcal{T}_\beta}^{\text{R}}$  with very high precision if one wanted to use directly Eq. (A1) for the determination of the magnetocrystalline anisotropy.

In the absence of SOI, we have  $H_{\text{SOI}} = 0$  and Eq. (A9) simplifies to  $\mathcal{T}_\beta = i[H, \sigma_\beta]/2$ . Since  $|\psi_{kn}\rangle$  is an eigenstate of  $H$  it follows that  $\langle \psi_{kn} | \mathcal{T}_\beta | \psi_{kn} \rangle = 0$  and therefore the last term in Eq. (A7) vanishes. Thus, in the absence of SOI, Eq. (A7) can be written as

$$G_{\mathcal{T}_\alpha\mathcal{T}_\beta}^{\text{R}} = \frac{\hbar}{\mathcal{N}} \sum_{kn} f_{kn} \text{Im} \langle \psi_{kn} | \mathcal{T}_\alpha \sigma_\beta | \psi_{kn} \rangle. \quad (\text{A11})$$

Using  $\sigma_\alpha \sigma_\beta = \delta_{\alpha\beta} + i\epsilon_{\alpha\beta\gamma}\sigma_\gamma$ , one can derive Eq. (44) from (A11).

- [1] L. Berger, *Phys. Rev. B* **33**, 1572 (1986).
- [2] G. E. Volovik, *J. Phys. C: Solid State Phys.* **20**, L83 (1987).
- [3] S. E. Barnes and S. Maekawa, *Phys. Rev. Lett.* **98**, 246601 (2007).
- [4] K.-J. Lee, M. D. Stiles, H.-W. Lee, J.-H. Moon, K.-W. Kim, and S.-W. Lee, *Phys. Rep.* **531**, 89 (2013).
- [5] S. A. Yang, G. S. D. Beach, C. Knutson, D. Xiao, Q. Niu, M. Tsoi, and J. L. Erskine, *Phys. Rev. Lett.* **102**, 067201 (2009).
- [6] T. Schulz, R. Ritz, A. Bauer, M. Halder, M. Wagner, C. Franz, C. Pfleiderer, K. Everschor, M. Garst, and A. Rosch, *Nat. Phys.* **8**, 301 (2012).
- [7] K.-W. Kim, J.-H. Moon, K.-J. Lee, and H.-W. Lee, *Phys. Rev. Lett.* **108**, 217202 (2012).
- [8] G. Tatara, N. Nakabayashi, and K.-J. Lee, *Phys. Rev. B* **87**, 054403 (2013).
- [9] I. Garate and A. H. MacDonald, *Phys. Rev. B* **80**, 134403 (2009).
- [10] A. Manchon and S. Zhang, *Phys. Rev. B* **79**, 094422 (2009).
- [11] D. A. Pesin and A. H. MacDonald, *Phys. Rev. B* **86**, 014416 (2012).
- [12] E. van der Bijl and R. A. Duine, *Phys. Rev. B* **86**, 094406 (2012).
- [13] X. Wang and A. Manchon, *Phys. Rev. Lett.* **108**, 117201 (2012).
- [14] P. M. Haney, H.-W. Lee, K.-J. Lee, A. Manchon, and M. D. Stiles, *Phys. Rev. B* **87**, 174411 (2013).
- [15] P. M. Haney, H.-W. Lee, K.-J. Lee, A. Manchon, and M. D. Stiles, *Phys. Rev. B* **88**, 214417 (2013).
- [16] K. M. D. Hals and A. Brataas, *Phys. Rev. B* **88**, 085423 (2013).
- [17] K.-W. Kim, S.-M. Seo, J. Ryu, K.-J. Lee, and H.-W. Lee, *Phys. Rev. B* **85**, 180404 (2012).
- [18] C. Ciccarelli, K. M. D. Hals, A. Irvine, V. Novak, Y. Tserkovnyak, H. Kurebayashi, A. Brataas, and A. Ferguson, *Nat. Nanotechnol.* **10**, 50 (2014).
- [19] K. M. D. Hals and A. Brataas, *Phys. Rev. B* **91**, 214401 (2015).
- [20] I. Mihai Miron, G. Gaudin, S. Auffret, B. Rodmacq, A. Schuhl, S. Pizzini, J. Vogel, and P. Gambardella, *Nat. Mater.* **9**, 230 (2010).
- [21] I. Mihai Miron, K. Garello, G. Gaudin, P.-J. Zermatten, M. V. Costache, S. Auffret, S. Bandiera, B. Rodmacq, A. Schuhl, and P. Gambardella, *Nature (London)* **476**, 189 (2011).
- [22] L. Liu, O. J. Lee, T. J. Gudmundsen, D. C. Ralph, and R. A. Buhrman, *Phys. Rev. Lett.* **109**, 096602 (2012).
- [23] L. Liu, C.-F. Pai, Y. Li, H. W. Tseng, D. C. Ralph, and R. A. Buhrman, *Science* **336**, 555 (2012).
- [24] K. Garello, I. M. Miron, C. O. Avci, F. Freimuth, Y. Mokrousov, S. Blügel, S. Auffret, O. Boulle, G. Gaudin, and P. Gambardella, *Nat. Nanotechnol.* **8**, 587 (2013).
- [25] J. Kim, J. Sinha, M. Hayashi, M. Yamanouchi, S. Fukami, T. Suzuki, S. Mitani, and H. Ohno, *Nat. Mater.* **12**, 240 (2013).
- [26] X. Qiu, P. Deorani, K. Narayanapillai, K.-S. Lee, K.-J. Lee, H.-W. Lee, and H. Yang, *Sci. Rep.* **4**, 4491 (2014).
- [27] C.-F. Pai, L. Liu, Y. Li, H. W. Tseng, D. C. Ralph, and R. A. Buhrman, *Appl. Phys. Lett.* **101**, 122404 (2012).
- [28] P. P. J. Haazen, E. Mure, J. H. Franken, R. Lavrijsen, H. J. M. Swagten, and B. Koopmans, *Nat. Mater.* **12**, 299 (2013).
- [29] L. Thomas, K. Ryu, S. Yang, and S. S. P. Parkin, *Nat. Nanotechnol.* **8**, 527 (2013).
- [30] S. Emori, U. Bauer, S. Ahn, E. Martinez, and G. S. D. Beach, *Nat. Mater.* **12**, 611 (2013).
- [31] F. Freimuth, S. Blügel, and Y. Mokrousov, *Phys. Rev. B* **90**, 174423 (2014).
- [32] R. Urban, G. Woltersdorf, and B. Heinrich, *Phys. Rev. Lett.* **87**, 217204 (2001).
- [33] Y. Tserkovnyak, A. Brataas, and G. E. W. Bauer, *Phys. Rev. Lett.* **88**, 117601 (2002).
- [34] O. Mosendz, J. E. Pearson, F. Y. Fradin, G. E. W. Bauer, S. D. Bader, and A. Hoffmann, *Phys. Rev. Lett.* **104**, 046601 (2010).
- [35] O. Mosendz, V. Vlaminc, J. E. Pearson, F. Y. Fradin, G. E. W. Bauer, S. D. Bader, and A. Hoffmann, *Phys. Rev. B* **82**, 214403 (2010).
- [36] F. D. Czeschka, L. Dreher, M. S. Brandt, M. Weiler, M. Althammer, I.-M. Imort, G. Reiss, A. Thomas, W. Schoch, W. Limmer *et al.*, *Phys. Rev. Lett.* **107**, 046601 (2011).
- [37] A. Azevedo, L. H. Vilela-Leao, R. L. Rodriguez-Suarez, A. F. Lacerda Santos, and S. M. Rezende, *Phys. Rev. B* **83**, 144402 (2011).
- [38] M. Weiler, M. Althammer, M. Schreier, J. Lotze, M. Pernpeintner, S. Meyer, H. Huebl, R. Gross, A. Kamra, J. Xiao *et al.*, *Phys. Rev. Lett.* **111**, 176601 (2013).
- [39] H. J. Jiao and G. E. W. Bauer, *Phys. Rev. Lett.* **110**, 217602 (2013).
- [40] D. Wei, M. Obstbaum, M. Ribow, C. H. Back, and G. Woltersdorf, *Nat. Commun.* **5**, 3768 (2014).
- [41] M. Weiler, J. M. Shaw, H. T. Nembach, and T. J. Silva, *Phys. Rev. Lett.* **113**, 157204 (2014).
- [42] C. Hahn, G. de Loubens, M. Viret, O. Klein, V. V. Naletov, and J. Ben Youssef, *Phys. Rev. Lett.* **111**, 217204 (2013).
- [43] R. A. Duine, *Phys. Rev. B* **79**, 014407 (2009).
- [44] Y. Tserkovnyak and S. A. Bender, *Phys. Rev. B* **90**, 014428 (2014).
- [45] F. Freimuth, S. Blügel, and Y. Mokrousov, *J. Phys.: Condens. Matter* **26**, 104202 (2014).
- [46] F. Freimuth, R. Bamler, Y. Mokrousov, and A. Rosch, *Phys. Rev. B* **88**, 214409 (2013).
- [47] H. Ebert, S. Mankovsky, D. Ködderitzsch, and P. J. Kelly, *Phys. Rev. Lett.* **107**, 066603 (2011).
- [48] Z. Qian and G. Vignale, *Phys. Rev. Lett.* **88**, 056404 (2002).
- [49] R. R. Birss, *Symmetry and Magnetism* (North-Holland, Amsterdam, 1964).
- [50] I. Garate and A. MacDonald, *Phys. Rev. B* **79**, 064403 (2009).
- [51] K. Ando, T. Yoshino, and E. Saitoh, *Appl. Phys. Lett.* **94**, 152509 (2009).
- [52] M. Gradhand, D. V. Fedorov, P. Zahn, I. Mertig, Y. Otani, Y. Niimi, L. Vila, and A. Fert, *SPIN* **02**, 1250010 (2012).
- [53] W. Zhang, M. B. Jungfleisch, W. Jiang, Y. Liu, J. E. Pearson, S. G. E. t. Velthuis, A. Hoffmann, F. Freimuth, and Y. Mokrousov, *Phys. Rev. B* **91**, 115316 (2015).
- [54] A. Vedyayev, N. Ryzhanova, N. Strelkov, and B. Dieny, *Phys. Rev. Lett.* **110**, 247204 (2013).
- [55] T. Nan, S. Emori, C. T. Boone, X. Wang, T. M. Oxholm, J. G. Jones, B. M. Howe, G. J. Brown, and N. X. Sun, *Phys. Rev. B* **91**, 214416 (2015).
- [56] W. Zhang, W. Han, X. Jiang, S.-H. Yang, and S. S. P. Parkin, *Nat. Phys.* **11**, 496 (2015).
- [57] G. Géranton, F. Freimuth, S. Blügel, and Y. Mokrousov, *Phys. Rev. B* **91**, 014417 (2015).
- [58] K. Gilmore, Y. U. Idzerda, and M. D. Stiles, *Phys. Rev. Lett.* **99**, 027204 (2007).

- [59] J. Kuneš and V. Kamberský, *Phys. Rev. B* **65**, 212411 (2002).
- [60] F. Freimuth, Y. Mokrousov, D. Wortmann, S. Heinze, and S. Blügel, *Phys. Rev. B* **78**, 035120 (2008).
- [61] A. A. Mostofi, J. R. Yates, Y.-S. Lee, I. Souza, D. Vanderbilt, and N. Marzari, *Comput. Phys. Commun.* **178**, 685 (2008).
- [62] N. Marzari, A. A. Mostofi, J. R. Yates, I. Souza, and D. Vanderbilt, *Rev. Mod. Phys.* **84**, 1419 (2012).
- [63] M. Althammer, S. Meyer, H. Nakayama, M. Schreier, S. Altmannshofer, M. Weiler, H. Huebl, S. Geprägs, M. Opel, R. Gross *et al.*, *Phys. Rev. B* **87**, 224401 (2013).
- [64] W. Zhang, V. Vlaminc, J. E. Pearson, R. Divan, S. D. Bader, and A. Hoffmann, *Appl. Phys. Lett.* **103**, 242414 (2013).
- [65] V. Edelstein, *Solid State Commun.* **73**, 233 (1990).
- [66] A. Chernyshov, M. Overby, X. Liu, J. K. Furdyna, Y. Lyanda-Geller, and L. P. Rokhinson, *Nat. Phys.* **5**, 656 (2009).